International Journal of Machine Tools & Manufacture 51 (2011) 250–280

Contents lists available at ScienceDirect

International Journal of Machine Tools & Manufacture

journal homepage: www.elsevier.com/locate/ijmactool

Machining induced surface integrity in titanium and nickel alloys: A review

Durul Ulutan, Tugrul Ozel *

Manufacturing Automation Research Laboratory, Department of Industrial and Systems Engineering, Rutgers University, 96 Frelinghuysen Road, Piscataway, NJ 08854, USA

ARTICLE INFO

Article history:
Received 27 September 2010
Received in revised form
2 November 2010
Accepted 3 November 2010
Available online 24 November 2010

Keywords:
Machining
Surface integrity
Titanium alloys
Nickel alloys

ABSTRACT

Titanium and nickel alloys represent a significant metal portion of the aircraft structural and engine components. When these critical structural components in aerospace industry are manufactured with the objective to reach high reliability levels, surface integrity is one of the most relevant parameters used for evaluating the quality of finish machined surfaces. The residual stresses and surface alteration (white etch layer and depth of work hardening) induced by machining of titanium alloys and nickel-based alloys are very critical due to safety and sustainability concerns.

This review paper provides an overview of machining induced surface integrity in titanium and nickel alloys. There are many different types of surface integrity problems reported in literature, and among these, residual stresses, white layer and work hardening layers, as well as microstructural alterations can be studied in order to improve surface qualities of end products. Many parameters affect the surface quality of workpieces, and cutting speed, feed rate, depth of cut, tool geometry and preparation, tool wear, and workpiece properties are among the most important ones worth to investigate. Experimental and empirical studies as well as analytical and Finite Element modeling based approaches are offered in order to better understand machining induced surface integrity. In the current state-of-the-art however, a comprehensive and systematic modeling approach based on the process physics and applicable to the industrial processes is still missing. It is concluded that further modeling studies are needed to create predictive physics-based models that is in good agreement with reliable experiments, while explaining the effects of many parameters, for machining of titanium alloys and nickel-based alloys.

Contents

* Corresponding author. Tel.: +1 732 445 1099; fax: +1 732 445 5467.
E-mail address: ozel@rci.rutgers.edu (T. Ozel).

0890-6955/$ - see front matter © 2010 Elsevier Ltd. All rights reserved.
doi:10.1016/j.ijmachtools.2010.11.003

1. Introduction

The quality and performance of a product is directly related to surface integrity achieved by final machining. Surface integrity includes the mechanical properties (residual stresses, hardness etc.), metallurgical states (phase transformation, microstructure and related property variations, etc.) of the work material during processing and topological parameters (surface finish and other characteristic surface topographical features). When critical structural components in aerospace industry are machined with the objective to reach high reliability levels, surface integrity is one of the most relevant parameters used for evaluating the quality of machined surface. The residual stresses induced by machining of titanium alloys and nickel-based alloys are very critical due to safety and sustainability concerns.

Titanium alloys (e.g. Ti–5Al–2.55n (alpha), Ti–13V–11Cr–3AL (beta) or Ti–6Al–4V (alpha beta)) offer high strength-to-weight ratio, high toughness, superb corrosion and creep resistance, and biocompatibility and are used mainly in aerospace (e.g. jet engine sections in Fig. 1), gas turbine, rocket, nuclear, chemical vessels and increasingly in biomedical applications. On the other hand, nickel alloys (Ni–Co–Cr, Ni–Fe–Cr or Ni–Co–Fe) have the ability to retain most of their strength even after long exposures to extremely high temperatures and are the only material of choice for turbine sections of the jet engines. Nickel alloys are typically available wrought, forged, cast and in sintered (powder metallurgy) forms and often used in the hot sections of mission critical components in jet engines or gas turbine engines. For example, 50% weight of a jet engine is Inconel-718 (IN-718), a Ni–Fe–Cr alloy. This alloy exhibits very high strength and high temperature resistance, but it is difficult to machine this alloy due to these properties, causing low tool life for the tools to machine it [1]. On the other hand, Inconel 100 (IN-100), a Ni–Co–Cr superalloy, is used mainly for parts operating at intermediate temperature regimes, for components such as disks, spacers and seals. Cast nickel-based alloys are also used for turbine and compression blades in hot sections of jet engines.

Due to high toughness and work hardening behavior of these alloys, machining is generally extremely difficult. Several research studies has been reported in literature addressing the issues related to machining of nickel-based alloys such as rapid tool wear and undesirable alteration of machined surfaces as workpiece easily forms a work-hardened layer in response to the machining induced strain loading on the sub-surface. The low thermal conductivity of such alloys often leads to increased temperatures at the tool cutting edge and results in adhesion of workpiece material to the cutting edge and presence of hard abrasive particles in alloys structure creating accelerated tool wear. The high localized heat, increased temperatures, temperature gradients and high pressure induced stresses also cause microstructure changes creating white-layer/surface damage within the material in-depth direction and may cause detrimental effects on the performance of the machined part.

2. 2. Workpiece materials and applications

There are many different workpiece materials mainly used in aerospace industry that can be grouped into two parts: titanium and its alloys and nickel-based super alloys.

2.1. Titanium-based alloys

The use of titanium and its alloys has increased recently, because of their superior properties and improvements in machinability of these alloys. Main strengths of titanium-based alloys are their low density (nickel-based alloys are twice denser than titanium-based alloys), high strength at elevated temperatures, and high corrosion and creep resistance, as well as toughness, durability, and biological compatibility [2–4].

Different titanium alloys have been used for studies, such as Ti–6Al–4V (Ti-64) [5–11], Ti–6Al–2Sn–4Zr–2Mo–0.08Si (Ti–6242S) [12–14], Ti–6Al–2Sn–4Zr–6Mo (Ti–6246) [15], Ti–5.8Al–4Sn–3.5Zr–0.7Nb–0.5Mo–0.35Si–0.06C (Ti–834) [11,16], Ti–4.5Al–2Nb–2Mn–0.8%TiB_2 (Ti-45-2-2 XD) [17,18], Ti–4.5Al–4.5Mn [19], Ti–6Al–6V–2Sn (Ti-6-6-2) [20], Ti–5Al–4Mo–2Sn–6Si–2Fe (TA-48) [21], and Ti–6Al–7Nb [22], as shown in Table 1. The quality of surface integrity has been identified as one of the most important

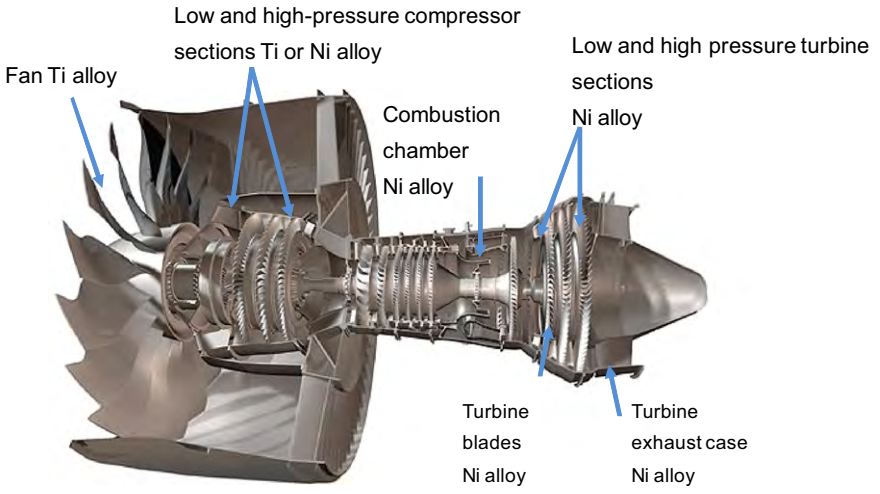

Fig. 1. Cross section of a jet engine (courtesy of Pratt and Whitney).

Table 1
Materials, their different alloys and studies appeared in the literature.

Material	Alloys	References
Titanium	Ti-64	Chen et al. [5], Che-Haron and Jawaid [6], Wang et al. [7], Nurul-Amin et al. [8], Sun et al. [9], Sun and Guo [10], Thomas et al. [11]
	Ti-6242S	Che-Haron et al. [12], Ginting and Nouari [13], Ginting and Nouari [14]
	Ti-6246	Che-Haron [15]
	Ti-834	Sridhar et al. [16], Thomas et al. [11]
	Ti-45-2-2 XD	Mantle and Aspinwall [17], Mantle and Aspinwall [18]
	Ti-4.5Al-4.5Mn	Zoya and Krishnamurthy [19]
	Ti-6-6-2	Kitagawa et al. [20]
	TA-48	Nabhani [21]
	Ti-6Al-7Nb	Cui et al. [22]
Nickel	IN-718	Sadat [24], Sadat et al. [25], Ezugwu and Tang [26], Liao and Shiue [27], Derrien and Vigneau [28], Kitagawa et al. [20], Rahman et al. [29], Ezugwu et al. [30], Darwish [31], Guerville and Vigneau [37], Li et al. [32], Schlauer et al. [33], Arunachalam et al. [34,35], Coelho et al. [36], Dudzinski et al. [38], Mitrofanov et al. [39], Sharman et al. [1,40,41], Zhang et al. [42], Axinte et al. [43], Aspinwall et al. [44], Pawade et al. [45], Uhlmann et al. [46], Outeiro et al. [47], Pawade et al. [48], Courbon et al. [49], Jemielniak [50], Lorentzon et al. [51], Lu and Guo [52], Pawade et al. [53], Ranganath et al. [54]
	NiCr20TiAl	Zou et al. [55]
	IN-100	Ranganath et al. [56]
	IN-738LC	Österle and Li [57]
	UDIMET 720LI	Cui et al. [58], Joshi et al. [59]
	Nimonic 75 & 105	Wright and Chow [60]

issues in titanium machining [6,15,17,18], as it is also one of the major challenges besides the machinability of the workpieces [19,23] and wear of the tools [7]. It is observed that compared to the most famous nickel alloy IN-718, titanium alloy Ti–6Al–6V–2Sn offered considerably higher machinability and lower temperature outcomes [20].

2.2. Nickel-based alloys

Nickel-based alloys are also very popular in the industry due to their advantages over titanium-based alloys. The main strengths of the nickel-based alloys are being heat-resistant, retaining their high mechanical and chemical properties at high temperatures, and having high melting temperatures, high corrosion resistance, as well as resistance to thermal fatigue, thermal shock, creep, and erosion [2–4]. Among nickel-based alloys, IN-718 is the most widely used alloy and because of that it has been studied extensively for the analysis of surface integrity, residual stress and machinability [1,20,26–54]. The machining studies are not limited to IN-718 include other nickel-based alloys. Surface damage on the NiCr20TiAl nickel-based alloy during turning processes were reported [55]. Another nickel-based alloy IN-100 was the material used in the finite element analysis of white layer formation [56], while another study used In-738LC in order to observe white layer formation experimentally [57]. Researchers worked with another nickel-based alloy UDIMET 720LI on the microstructure and yield strength of the material as well as residual stresses, hardness profiles, and surface roughness during milling [58,59], and Nimonic 75 & 105 alloys for their thermal and mechanical responses to turning process [60].

2.3. Aerospace and power industries

In aerospace industry, the materials mostly used are nickel and titanium, and their alloys, instead of steel [61], and when steel is used, it is generally austenitic stainless steel [3]. They have better strength at low and high temperatures, they are more resistant to wear and chemical degradation, which make them favorable. However, their poor thermal properties also prevent from producing good surface results at elevated temperatures due to deformation and friction induced heat and microstructural changes, which is why improving their surface integrity properties during machining is important.

It is reported that nickel-based alloys compose over half of the materials used in the aerospace industry, and aero engines utilize IN-718 material greatly [34]. These alloys are under constant improvement for better strength and surface integrity. For example, UDIMET 720LI, a nickel-base superalloy widely used in aerospace industry, with addition of Co–Ti to the composition might make this alloy become more useful for the aerospace industry, by increased yield strength and potentially better surface quality [58]. The significant challenges faced are that Nickel-based heat-resistant alloys have low thermal conductivity that increases the thermal effects during machining, they often exhibit work-hardening behavior, high adhesion characteristic onto the tool face altering process parameters completely, may contain hard abrasive particles and carbides that create excessive tool wear, and hence the surface quality of the end products can be disappointing [43].

On the other hand, titanium alloys such as Ti-45-2-2 XD [17,18] and Ti-6242S [13] are known to be widely used in aerospace materials such as compressor and turbine blades. The strength-to-weight ratio that titanium alloys has to offer, as well as their strength in corrosion resistance and high strength under high temperature conditions make these alloys very attractive for the aerospace industry [9]. The aircrafts of the near future are considered to use excessive amounts of carbon fiber compounds that utilize titanium and its alloys, especially if the machinability and productivity of these alloys can be increased via studies on their properties and the interactions between those and tool materials [11].

Consequently, the aerospace industry generally benefits from the superior material properties of titanium and nickel materials and their alloys instead of steel materials, especially their high mechanical and thermal resistances and thermal conductivity, as well as the lightweight of titanium.

2.4. Biomedical industry

The use of various materials such as polymers, metals, ceramics, and composites in biomedical devices has been widespread [62]. Within these materials, the use of titanium alloys, nickel alloys, nickel–titanium alloys, and composites are heavily investigated. In particular, nickel–titanium alloys have attracted research interest

in this area, because of their superelasticity and shape memory properties, and their compatibility in terms of bioactivity [63]. The release of the nickel ion was found to be very toxic, so coating types were studied in order to restrain this release and improve the biomimetic surface [64]. The biocompatibility of these materials were studied, and when a coating layer that consists of octacalcium phosphate and hydroxyapatite was applied to the material, the biocompatibility of the material was found to improve due to increasing cytokine release and the increase in the number of adherent cells to the material [64].

A titanium-based alloy, Ti–6Al–7Nb was investigated in order to find its high temperature deformation behavior [22], and researchers found that during hot deformation of Ti–6Al–7Nb at around 750–850 °C and at low strain rates, dynamic recrystallization of the α-phase was observed. When they increased both the temperature and the strain rate, however, the material showed a flow localization and dynamic recovery in β-phase [22]. The use of Nb as the β-stabilizer instead of vanadium was due to the fact that Vanadium is a toxic material that cannot be allowed in biomedical devices.

The nickel–titanium alloys based on Nitinol (NiTi) is also widely used because of their shape memory property. Machining these alloys was found to be very difficult, owing to their high ductility and work hardening behavior [65]. It was suggested that for these materials, the tool wear is high whether the feed rate and cutting speed are high or low, so increasing the material removal rate while taking care of the surface quality by rapid tool changing was recommended [65]. Micro-milling was proposed as a favorable method to machine these materials, and using a minimum quantity of lubrication was suggested for increased surface quality [66]. When micro-milling at $V=33$ m/min, $f=6$–30 μm/tooth, $DoC=10$–100 μm, and width of cut $=250$ μm, where V is the cutting speed, f is the feed rate, and DoC is the depth of cut, a high feed rate and a relatively high width of cut were found to form better chips, which extended tool life and enhanced the workpiece quality [66]. Tool coating was suggested rather than using uncoated tools, but multi-layer TiCN/TiAlN or TiCN/TiN coated cemented carbide tools were found to provide better results compared to PCD or CBN tools in turning and drilling processes in terms of workpiece quality and tool costs [67].

These types of materials can be extremely useful for the biomedical industry, because of their improved properties. They can be used in biomedical devices such as stents, dental implants, orthopedic implants, and other devices, and their high biocompatibility with the human body is a significant concern.

3. Surface integrity

Surface conditions of a manufacturing/machining metal part directly influence the processing and end use of that part. These influences can be categorized as (a) frictional and wear behavior at the interfaces of bodies in contact, (b) effectiveness and control of lubrication during processing (forging, stamping, rolling) and in end use (bearing, shafts, all rotating and moving elements), (c) appearance and the role of the surface in subsequent surface finishing operations (cleaning, coating, or surface treating), (d) initiation of surface cracks and residual stresses that influence fatigue life and corrosion properties [68], and (e) heat transfer and electrical conductivity between two bodies contacting each other.

A typical of the surface of metals includes a contaminated thin layer (1–10 nm), an oxidation layer (10–100 nm) followed by a work-hardened layer whose thickness depends on material processing conditions and the environment. Unless the metal is processed and kept in an inert (oxygen free) environment, or it is a noble metal, an oxide layer usually develops on top of the work-hardened or amorphous layer [69]. At microscale the surface layer of a manufactured part is not smooth and may show various different features: microcracks, craters, folds, laps, seams, inclusions, plastic deformation, residual stresses, oxide layer, metallurgical transformations (heat affected zone, decarburization, recast layer, phase transformations, alloy depletion). The surface layer characteristics that can change through processing include plastic deformation, residual stresses, cracks, hardness, overaging, phase changes, recrystallization, intergranular attack, and hydrogen embrittlement. When a machining process is applied, the surface layer sustains local plastic deformation.

The surface integrity of the final part is crucial in machining processes. In most applications, having the smoothest possible surface is desired, especially when the fatigue life of a machined part is important [70]. However, in some cases, having a rougher surface can be preferred. These cases generally occur in the biomedical field [63].

Machining processes induce and affect various surface integrity attributes on the finished parts. These can be grouped as: (a) topography characteristics such as textures, waviness and surface roughness, (b) mechanical properties affected such as residual stresses and hardness, and (c) metallurgical state such as microstructure, phase transformation, grain size and shape, inclusions etc. These alterations of surface are considered in five groups to mechanical, thermal, metallurgical, chemical, and electrical properties [71].

There are many studies on the issue of surface integrity of machined parts, and an extensive review of such studies has already been done [3,4]. However, this study includes a review of various surface integrity problems with the effect of many cutting parameters, using titanium and nickel alloys and many different tool materials.

3.1. Surface defects

There are many forms of surface defects reported in the literature. As depicted in Figs. 2–5, main forms are surface drag, material pull-out/cracking, feed marks, adhered material particles, tearing surface, chip layer formation, debris of microchips, surface plucking, deformed grains, surface cavities, slip zones, laps (material folded onto the surface), and lay patterns [1,14,17,38,43,45,48,54,55,71]. It has been reported that when the thermal softening of the material is increased, compressive stresses also increase and such surface flaws clear out of the machined surface, as well as enabling the workpiece near-surface to reconstruct itself easily [45]. These types of defects were observed by different researchers in many different nickel- and titanium-alloys such as NiCr20TiAl [55], IN-718 [1,38,45,48,54], RR_x powder based nickel alloy [43] Ti-6242S [14] and Ti-64 [6].

The cutting parameters can affect these defects to some degree. Feed marks are effective in machining, but their severity can be altered by varying and optimizing the feed rate [14]. Cutting speed values can affect the amount of microchip debris on the surface, and material plucking, tearing, dragging, and smearing can be affected by depth of cut among other parameters [14]. During machining of nickel and titanium alloys, such problems can be problematic, so optimizing the cutting conditions is essential [55].

There are many surface defects that can be found in machining processes, especially when investigated in micron precisions. The main surface defects are considered to be feed marks, chip redeposition to the surface, and grain deformations, since these are the ones in the biggest scale among the surface defects. Also, plucking of particles from the surface and their redeposition to the surface create two different defects, whereas these particles can also cause dragging and tearing defects on the next pass from the surface. Adjusting cutting parameters according to these defects is very hard, and even then, a complete elimination is not possible.

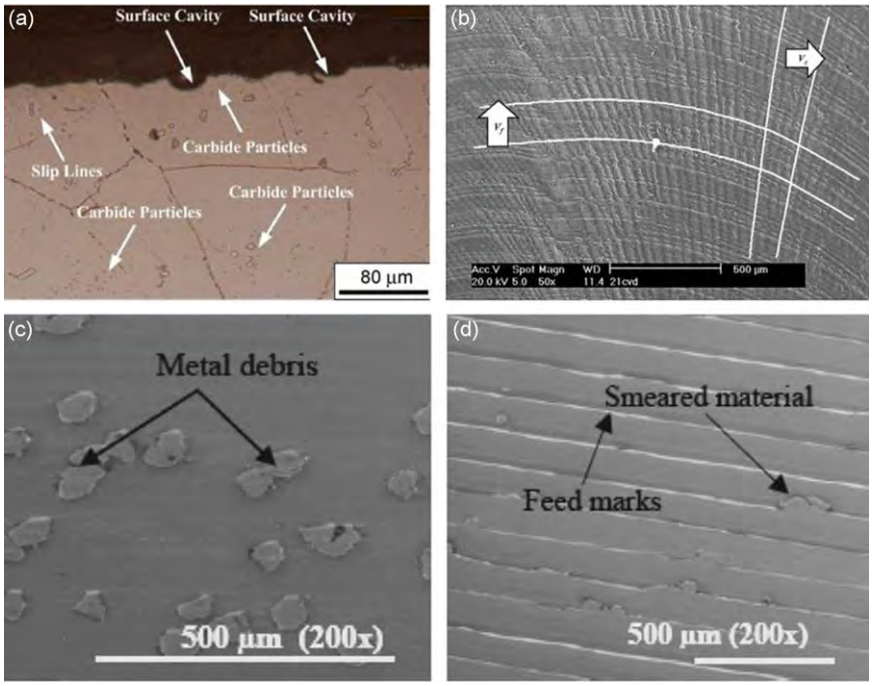

Fig. 2. Surface damages in machining of nickel- and titanium-based alloys: (a) Metallographical microstructure of NiCr20TiAl after turning at $V=60$ m/min, $f=0.15$ mm/rev and $DoC=1$ mm [55], (b) lay pattern after dry milling Ti-6242S at $V=125$ m/min, $f=0.2$ mm/tooth, $DoC=2.5$ mm [14], (c) metal debris after turning IN-718 at $V=125$ m/min, $f=0.05$ mm/rev, and $DoC=0.5$ mm [45], and (d) smeared material and feed marks after turning IN-718 at $V=125$ m/min, $f=0.1$ mm/rev, and $DoC=0.75$ mm [45].

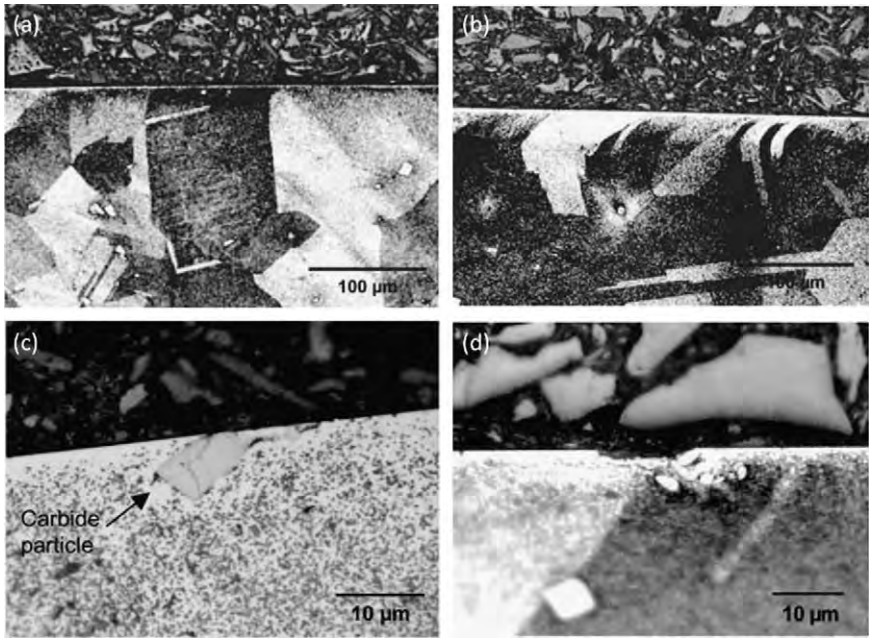

Fig. 3. Surface defects in turning IN-718 with $V=40$–120 m/min, $f=$ 0.15–0.25 mm/rev, $DoC=0.25$ mm: microstructural deformations in (a) new tool and (b) worn tool, (c) carbide cracking in the deformed layer, and (d) surface tearing and cavities [1].

Many workpiece materials include carbide particles in their structure. Also, many coating materials involve some carbide in them. As the tool wears, and the workpiece is machined, these carbide particles are sometimes removed from the machined surface or the tool and get stuck on the workpiece surface [55]. This phenomenon is called carbide cracking, and it causes a sudden increase in the shear stress during cutting that leads to surface cavities due to plucking. This process causes residual cavities and cracks to be formed inside the machined surface, causing even further problems.

Titanium and nickel alloys are both prone to carbide cracking where the existence of crack locations make the fatigue life of the material to decrease substantially [54]. These materials are strengthened by carbides such as titanium carbide (TiC0 and niobium carbide (NbC). When feed rates and depth of cut values lower than 50 μm are used to observe the possibility of good surface roughness, the carbide particles from these strengthening pieces were observed to crack from the surface and be smeared to another part of the workpiece material to create surface integrity problems. Since the sizes of these carbide particles were also found

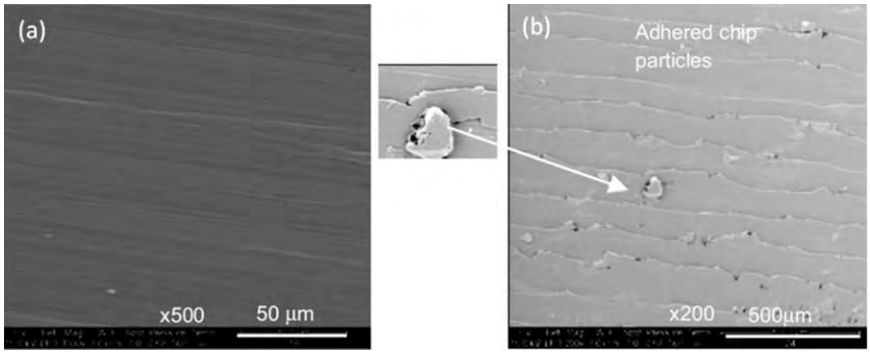

Fig. 4. (a) Feed marks (V=475 m/min, f=0.05 mm/rev, DoC=0.5 mm) and (b) adhered chip particles (V=475 m/min, f=0.1 mm, DoC=1 mm) after high speed turning of IN-718 [48].

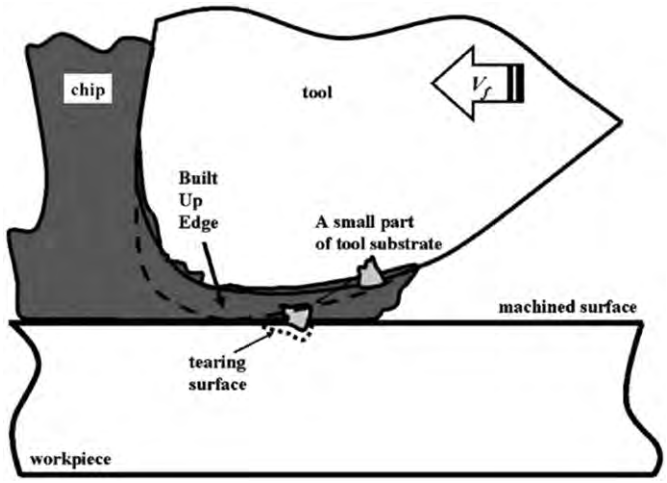

Fig. 5. Surface tearing mechanism in machining of Ti-6242S [14].

to be around 20 μm, comparable to the feed rate and depth of cut values (Fig. 6). Carbide particles as shown in Fig. 3c are considered to be unable to deform, which makes them to be removed completely at once, leaving cavities behind, as well as causing high oscillations in forces [1,55]. Hence, taking these possibilities in account and planning the machining accordingly is extremely important.

As a result, carbide cracking can be a serious problem in terms of micro-scale surface integrity. Especially when the depth of cut and feed values are very small, the carbide particle sizes become too close to a concerning level that carbide cracking might gain significant importance in the surface of the end product.

3.2. Microstructural alterations

During the machining operations, the workpiece material is exposed to thermal, mechanical, and chemical energy that can lead to strain aging and recrystallization of the material. Due to the strain aging process, the material might become harder but less ductile, and recrystallization might cause the material to become less hard but more ductile. These thermal (high temperature and rapid quenching) and mechanical (high stress and strain) effects are the main reasons for the microstructural alterations in the material, as well as phase transformations and plastic deformations [72].

Studies on Ti-64 and Ti-6246 showed that a very thin layer of plastic deformation was formed in the immediate sub-surface of the workpiece, and as the tool wears out, plastic deformation and subsequently the thickness of the deformed layer increased, due to microstructural alterations [1,6,15]. The depth of these microstructural alterations beneath the surface has been observed to increase when the cutting speed and feed rate are increased [1,14], and also prolonged machining with worn tools was found to increase microstructural alterations to the material in the form of severe plastic deformation and thicker 'disturbed' layer on the machined surface [15]. As shown in Fig. 7, the microstructure can be bent or strained up to 10 μm depth after end milling IN-718 at V=90 m/min, f=0.2 mm/tooth, and DoC=0.5 mm [44]. Turning IN-718 at V=40–120 m/min, f=0.15–0.25 mm/rev, DoC=0.25 mm is also found to deform the grain boundaries in the direction of machining (Fig. 8) [40], and increases in feed rate or tool wear were related to increasing microstructural alterations [1]. Fig. 9 also shows the amount of microstructural alterations in Ti-6242S alloy (a) before machining and (b) after milling at V=100 m/min, f=0.15 mm/tooth, and DoC=2 mm [14].

It is believed that these microstructural alterations can lead to white layer formation when strain aging is dominant, and when recrystallization is also observed, another layer of darker imagery under optical microscope that has a hardness value in between the white layer and the bulk material can be observed, which has been studied extensively for steel materials [73].

3.2.1. White layer formation

After the workpiece is machined, the surface exhibits different behavior than the interior of the bulk material. The microstructural alterations, thermomechanical processing in the material, phase changes (martensitic transformation and rapid cooling), and adhesion of chip particles cause the surface layer to exhibit different material behavior, which is generally harder than the bulk workpiece and which appears white under optical microscope, hence it is called the 'white layer'. It is sometimes accompanied by a 'dark layer' which exhibits material properties that are in between the white layer and the bulk workpiece material, and these layers are highly unpredictable. Sometimes, observing white layer formation is good for the application, but in many other applications, due to safety concerns, it is important to prevent its occurrence or at least predict how it would affect the end product, or remove it using post-processing techniques. White layer generally possesses fine grains, in some cases a nanocrystalline structure, it is harder than the bulk material but also it is brittle, while easing the crack development and propagation in the material [74], and it can also affect other measures of surface quality and the fatigue strength of the end product [75]. White layer was found to be 15% harder than the bulk material in IN-718, and polishing this type of zone of heavy localized deformation was

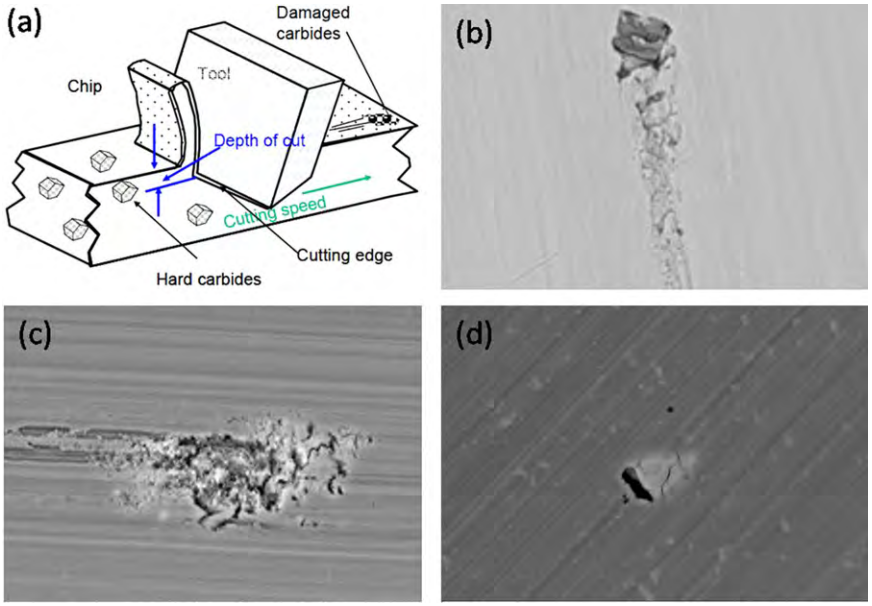

Fig. 6. How carbide particles can affect the surface quality: (a) carbide cracking, (b) dragging, (c) smearing, and (d) distributing marks on the machined surface of turned IN-718 [54].

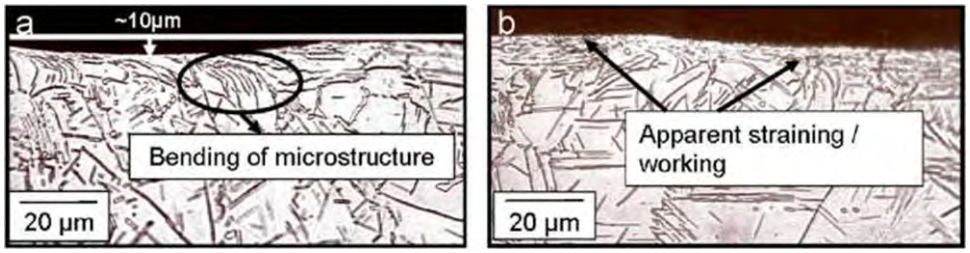

Fig. 7. Microstructural alterations in feed direction after end milling IN-718 at V=90 m/min, f=0.2 mm/tooth, and DoC=0.5 mm [44].

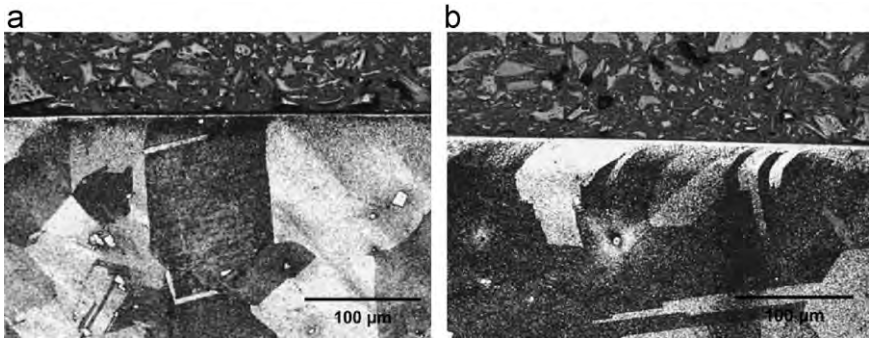

Fig. 8. Microstructural deformations of turned IN-718 at V=40–120 m/min, f=0.15–0.25 mm/rev, DoC=0.25 mm with (a) new tool and (b) worn tool [40].

found to decrease the thickness of this type of layer from 40 to 7–10 μm, while not changing its hardness [76].

Many research studies have been conducted to investigate white layer formation in turning of hardened steels [77–81]. According to their observations, white layers were results of high temperature gradients, plastic deformation, and flank wear land rubbing [75,78,82]. It is also believed that a quenching mechanism of rapid heating and cooling is very effective on creation of white and dark layers above the bulk material, as shown in Fig. 10. This quenching mechanism transforms the surface material from austenitic to martensitic structure, which plays the most important role in white layer formation [79]. However, it is also proven that in the absence of temperatures high enough to allow phase transformations, white layer formation still takes place, meaning that mechanical effects also play role in white layer formation.

The formation of white layers in machining titanium and nickel alloys is studied less extensively by researchers, although there are some valuable studies that contribute to surface integrity. It is

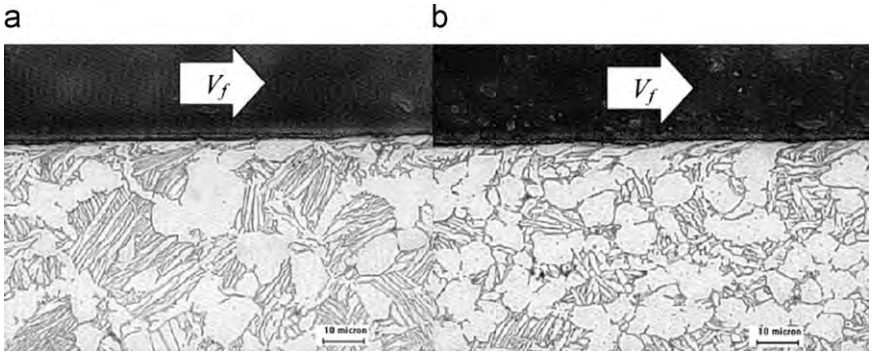

Fig. 9. Microstructural alterations in Ti-6242S after milling at $V=100$ m/min, $f=0.15$ mm/tooth, and $DoC=2$mm (a) at the beginning of machining and (b) after the tool wear of VB=0.3 mm [14].

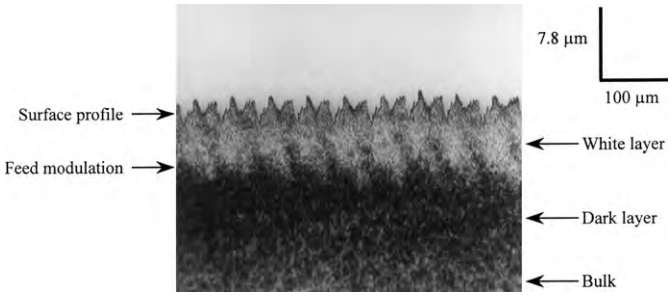

Fig. 10. Layers created after hard turning of steel [78].

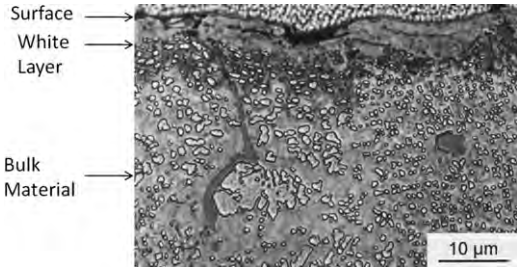

Fig. 11. Layers created after grinding IN-738LC [57].

claimed that especially under abusive machining conditions, a harder, or sometimes even softer white layer can be produced during machining titanium alloys [72,83]. Österle and Li [57] studied the white layer formation in grinding IN-738LC at $V=20$ m/s (Fig. 11), and claimed that rapid heating to the melting temperature (local melting of material) and subsequent quenching, as well as severe plastic deformation were the causes of this layer, which appeared in grey contrast in their pictures. They resemble this kind of white layer formation to a viscous fluid smearing over the machined surface, as the nanocrystalline structure of the white layer was found to have different size (50–100 nm diameter) equiaxed grains. It is also suggested that continuous dressing in grinding helped decrease the depth of the white layer formed on the surface. This white layer might cause microcracks to occur, which was suggested to be removed by subsequent fine grinding of the material.

In another study in turning of the nickel-based alloy RR_x that is obtained via powder metallurgy route at the cutting conditions of $V=175$–200 m/min, $f=0.15$–0.25 mm/rev, and $DoC=1$–2 mm, researchers found that white layer formation is the result of heat concentration at the immediate sub-surface section of the material due to machining conditions, and the low thermal conductivity of the nickel alloy RR_x enhance this effect [43]. Their findings showed that the observed white layer formation was only a few hundred nanometers deep into the surface, and no plastic deformation or microstructural alteration was observed other than this layer, at the initial stages of machining (Fig. 12). Che-Haron and Jawaid [6] claimed the opposite in their study on turning Ti-64 at $V=45$–100 m/min, $f=0.25$–0.35 mm/rev, and $DoC=2$ mm that the plastic deformation and microstructural alterations were observed at the end of the machining, and these deformations were believed to be the reason of white layer formation, while agreeing that at the initial stages of machining, no plastic deformation was observed. The thickness of such a layer was claimed to be less than 0.01 mm, even after dry machining at conventional cutting conditions for both Ti-6246 [15] and Ti-64 [6].

The white layer formation has been investigated from various points of view in the literature, and the main point agreed on is that white layer exhibits a smaller grain size than the bulk material and it is formed as a result of many different processes. These effects include plastic deformation, chemical reactions, high temperature gradients, rapid heating and cooling (quenching effect), thermal softening, mechanical effects, phase transformations, and microstructural alterations. These effects occur due to many parameters such as the cutting speed, feedrate, depth of cut, thermal conductivity of the tool and the workpiece, thus it is a complex phenomenon that needs special attention. It is known that the white layer thickness on the surface of the material is around 10–20 µm, so the measurement and validation of this property is difficult, which is the main reason of many different and contradicting findings appeared in the literature.

3.2.2. Plastic deformation

The main threats to surface integrity come from the plastic deformation of the workpiece during the machining process, and it is essential to study the effects of these deformations. It is known that these deformations are caused and/or supported by many parameters such as cutting parameters (cutting speed, feed, depth of cut), tool parameters (rake angle, edge radius, shape, coating, wear), and workpiece parameters (material, grain size). Many research studies have been conducted to find the main cause of the plastic deformations on the workpiece. It has been shown that as the tool wears, the plastic deformation on the workpiece increases during machining of titanium alloys Ti-64 and Ti-6246, which contributes in creation of white layers [6,15]. Also in machining nickel-alloy IN-718, it was found that although no significant plastic deformation was observed after 1 min of turning at $V=32$–56 m/min, $f=0.13$–0.25 mm/rev, $DoC=1,2$ mm, prolonged machining of 15 min showed severe plastic deformation at the immediate sub-surface of the material [30] (Fig. 13). Localized heating (thermal effects) and high stresses due

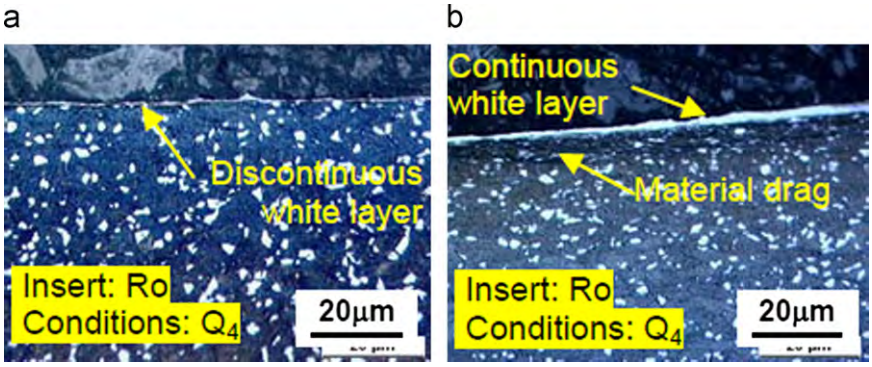

Fig. 12. White layers created after turning nickel-based alloy RR_x with (a) uniformly worn and (b) chipped ceramic tool at $V=175$–200 m/min, $f=0.15$–0.25 mm/rev, $DoC=1$–2 mm [43].

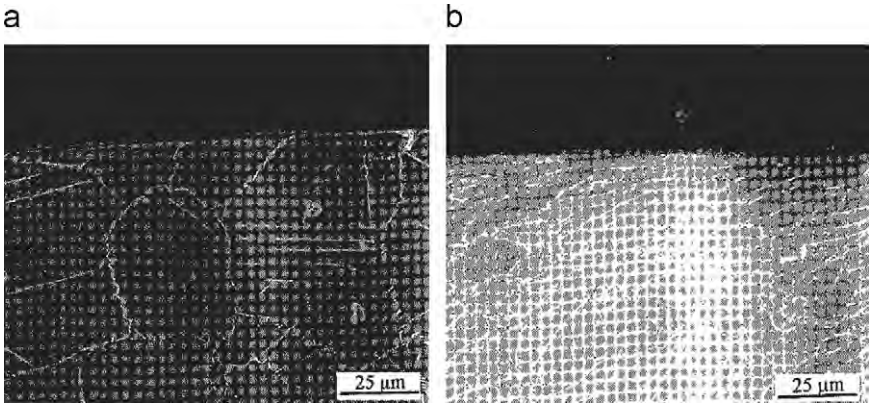

Fig. 13. Plastic deformation of surface layer of IN-718 after turning at $V=32$–56 m/min, $f=0.13$–0.25 mm/rev, and $DoC=1$, 2 mm for (a) 1 minute and (b) 15 min [30].

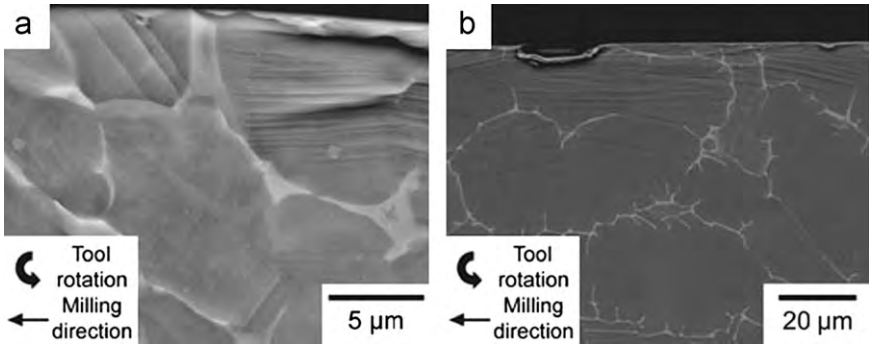

Fig. 14. Plastic deformation in the form of intense slip bands in milling (a) Ti-64 and (b) Ti-834 at $V=200$ m/min, $f=0.05$ mm/tooth, $DoC=1$ mm [11].

to increased forces (mechanical effects) are considered in combination for this change between the initial and the later stages of machining. The deformations and slip in the grain boundaries and elongation of grains indicate this severe plastic deformation, and the wear of the tool is the major reason in these deformations [30].

Occurrence of plastic deformation is not generally considered a problem itself as a surface integrity problem. It is also hard to measure or observe because it mainly occurs in the sub-surface of the material in a very short time and in a very narrow region of workpiece material. The main problem plastic deformation is known to cause is hardening of the surface of the workpiece because of excessive plastic strain and also residual stresses. It is found that both thermal and mechanical effects are significant in plastic deformations. It is believed that for facing IN-718 at $V=225$ m/min, $f=0.15$ mm/rev, mechanical effects are more dominant in plastic deformations closer to the surface by hardening the material, whereas thermal effects become more dominant in softening as it is deeper into the material [35]. In machining gamma-titanium aluminide, plastic deformation was found to be below 20 μm under the surface while milling at $V=70$–120 m/min, $f=0.06$–0.12 mm/tooth, $DoC=0.1$–0.5 mm [18], but with milling Ti-64 and Ti-834 alloys at $V=200$ m/min, $f=0.05$ mm/tooth, and $DoC=1$ mm, it was found to be around 30–50 μm [11]. As shown in Fig. 14, the plastic deformation in these cases were explained to be due to dislocation slip of the alpha phase [11]. Also with increasing

tool wear, plastic deformation increases, especially at lower cutting speeds such as 40 m/min [1] (Fig. 15). This can be explained by the fact that with increasing tool wear, the tool-workpiece contact area is increased due to reduced clearance angle on the tool, which creates more rubbing of the workpiece surface [41]. Very narrow regions of plastic deformations were observed in most cases [9], which show that plastic deformation is not the only factor for low surface qualities. It was shown that cutting conditions and tool wear are important factors on the plastic deformation of immediate sub-surfaces of machined parts after dry milling Ti-6242S at $V=100–125$ m/min, $f=0.15–0.2$ mm/tooth, and $DoC=2–2.5$ mm, and high pressure due to machining at high temperatures is the main cause of plastic deformation [14]. Increasing the cutting speed from 100 to 125 m/min and the feed rate from 0.15 to 0.2 mm/tooth increased the amount of plastic deformation, and when the tool wear increased from initial condition to VB=0.3 mm, the alteration of the microstructure was observed to be deeper [14]. On the contrary, it was shown by Sadat et al. [25] that when turning IN-718 at $V=0.2–1.61$ m/s, $DoC=0.028$ mm, increasing the cutting speed decreased the depth of plastic deformation.

3.3. Work hardening layer formation and microhardness

Workpiece surfaces are usually created by successive machining passes such as roughing, semi-finishing, and finishing. The characteristics of the machined surface layer created by the proceeding machining passes may have significant influence on the machining performance of the subsequent machining passes. This influence becomes more important for materials that exhibit high work-hardening behavior such as nickel alloys [52]. Workpiece easily forms a work-hardened layer in response to the machining induced deformations on the sub-surface. This is mainly due to work-hardening tendency of nickel alloys under excessive strain loading, creating a highly hardened surface layer and making it extremely difficult for the sequential cuts. Depth of cut in sequential cuts should be kept greater than the work-hardened layer which presents a difficult problem for industrial applications [52,84]. To overcome this problem, it is reported that continuously varying depth of cut helps improve machining nickel-based alloy RR_x [43].

The hardness of the material after being machined has been found to be greater on the surface of the material than through the depth of the material, where the heat and strain effects are neutralized for the bulk of the material. This is an evidence of work hardening during machining and a compressive layer [36]. These types of microhardness changes are also related to surface integrity issues, and have been studied by many researchers. Fig. 16 shows the microhardness profiles of IN-718 after turning at $V=500$ m/min, $f=0.1$ mm/rev, $DoC=0.35$ mm [36], and the drop from a higher surface hardness to a lower bulk material hardness is explained by the compressive layer due to work hardening of the material during machining. Fig. 17 shows the microhardness profiles of IN-718 after turning at $V=40–120$ m/min and $f=0.15–0.25$ mm/rev [1,40].

In machining superplastic materials such as IN-718, the work hardening behavior and the degree (or depth) of work hardening were reported mainly as signs of plastic deformation [48]. According to Pawade et al. [48], increasing cutting speed and depth of cut were found to decrease the depth of work hardening in turning IN-718 at $V=125–475$ m/min, $f=0.05–0.15$ mm/rev, $DoC=0.5–1$ mm, whereas increasing feed rate was claimed to increase the depth of work hardening (Fig. 18). For these materials, the hardening behavior is found to be mostly dependent on the grain size, and the flow softening is found to be mostly due to dynamic recovery, cavitation formation, grain refinement, and dynamic precipitation [42]. Another study on UDIMET 720 nickel alloy also showed that the microhardness of the material decreased from a maximum of 580 HV to 450 HV from the surface layer to a millimeter through the bulk material (Fig. 19), which can be the sign of creation of a "machining-affected zone" [59]. This machining-affected zone was depicted on turned Inconel-718 by Pawade et al. [48] at $V=125–475$ m/min, $f=0.05–0.15$ mm/rev, and $DoC=0.5–1$ mm (Fig. 20). Ezugwu and Tang [26] and Ezugwu et al. [30] also studied the effect of too wear on the microhardness profile when turning IN-718 at $V=152$ m/min, $f=0.125$ mm/rev, and

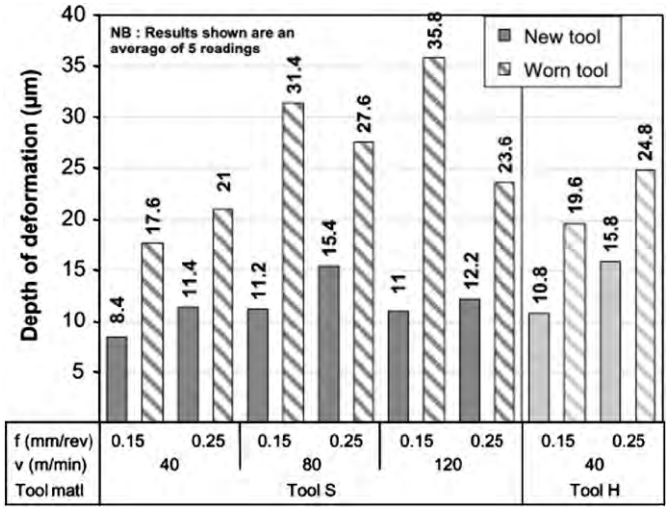

Fig. 15. Effects of machining parameters on the depth of microstructural deformation in turning IN-718 at $V=40–120$ m/min, $f=0.15–0.25$ mm/rev, $DoC=0.25$ mm [1].

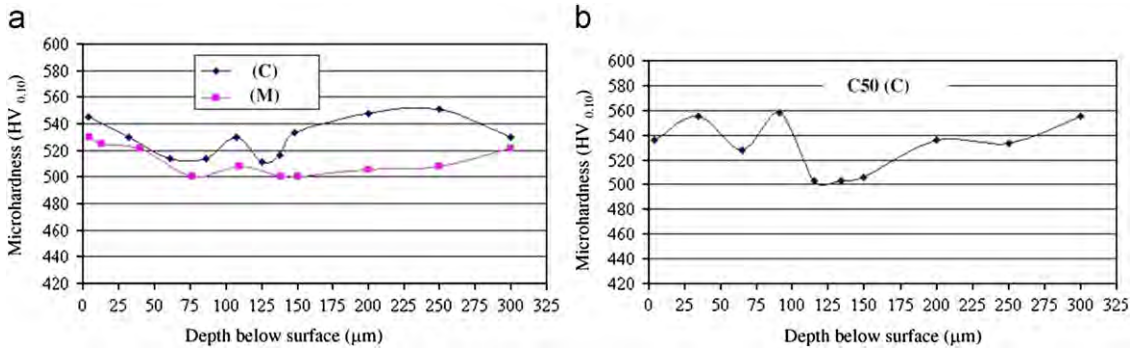

Fig. 16. Microhardness profiles through the depth of IN-718 after turning at $V=500$ m/min, $f=0.1$ mm/rev, and $DoC=0.35$ mm (C: commercial chamfer, M: modified chamfer) [36].

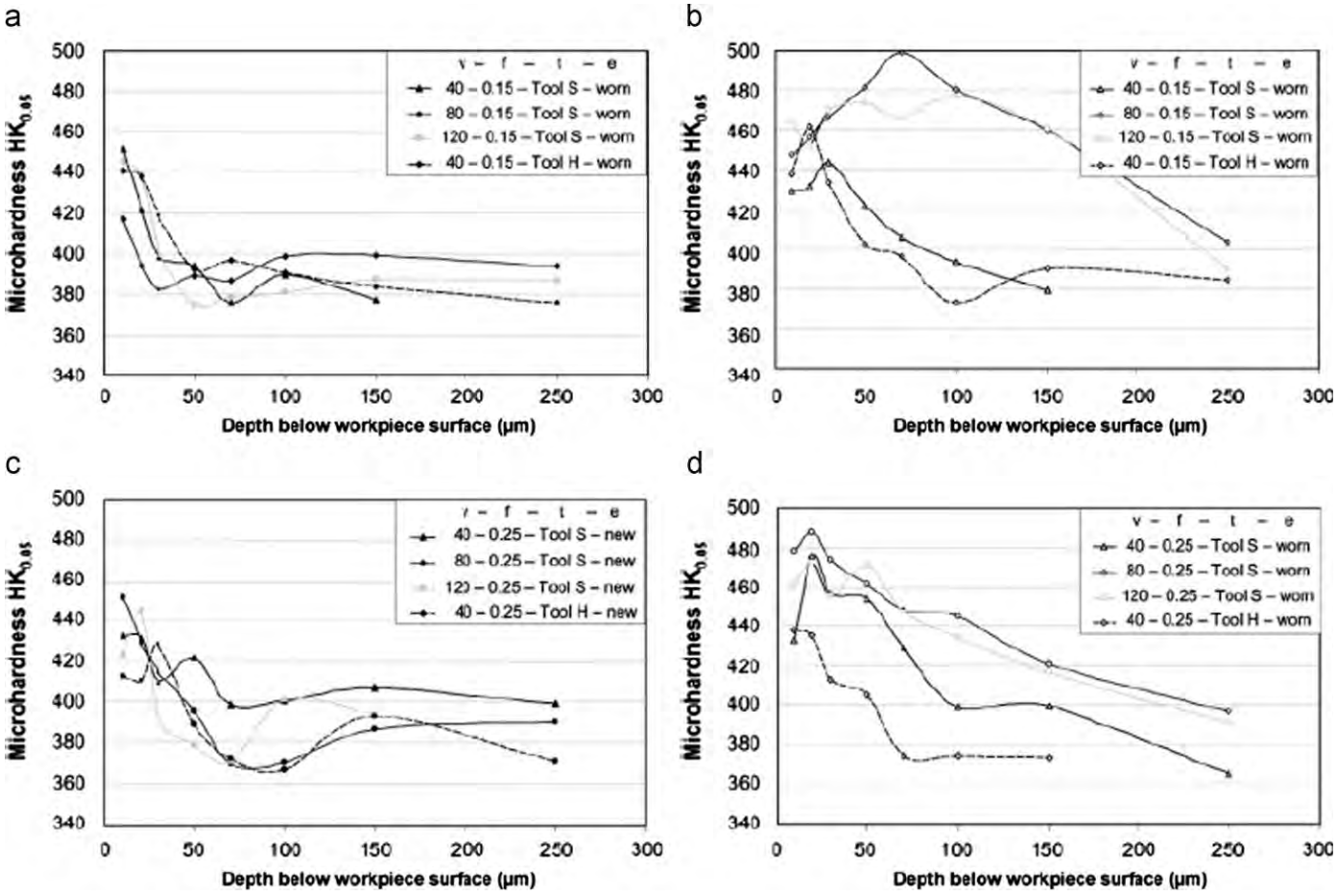

Fig. 17. Microhardness profiles through the depth of the material after turning IN-718 at V=40–120 m/min, f=0.15–0.25 mm/rev, and DoC=0.25 mm [1,40].

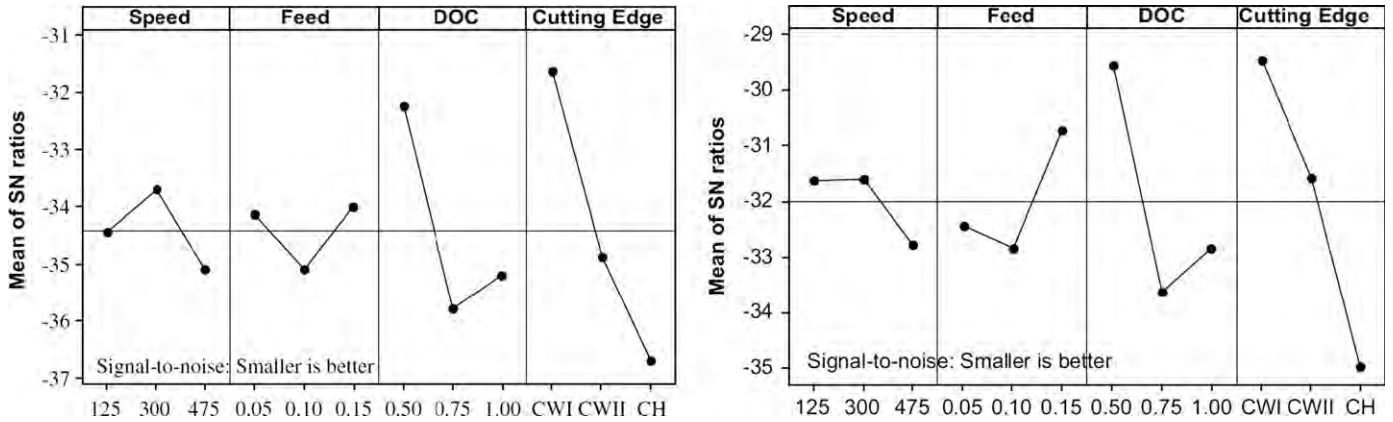

Fig. 18. Effect of all cutting parameters on the degree of work hardening in turning IN-718 at V=125–475 m/min, f=0.05–0.15 mm/rev, and DoC=0.5–1 mm [48].

DoC=2 mm, and at V=32–56 m/min, f=0.13–0.25 mm/rev, DoC=1–2 mm respectively, and found that at the start of machining, after 1 minute and after 3 min, microhardness decreases from surface to the depth of material (Figs. 21 and 22). They also found that, when the tool wear increases, the hardness of the material increases as well, due to the hardening process while turning (Figs. 21 and 22). Ezugwu et al.'s [30] study reveals that increasing feed rate and depth of cut in their work increased the microhardness of the material at both surface and sub-surface locations, as well as the depth of work-hardened zone (Fig. 22).

Also in turning Ti-64 at V=45–100 m/min, f=0.25–0.35 mm/rev, DoC=2 mm, Che-Haron and Jawaid [6] found similar results to the ones for IN-718. They showed that in the surface of turned Ti-64 at V=100 m/min, f=0.25–0.35 mm/rev, and DoC=2 mm, microhardness values are higher (~420 HV) than at the bulk material level (~340 HV), which they explain to be due to the work-hardening effect on the surface and the over-ageing of the sub-surface of the material due to very high cutting temperature (Fig. 23). They found that increasing the cutting speed created higher hardness values , while increasing the feed rate had a minimal effect [6].

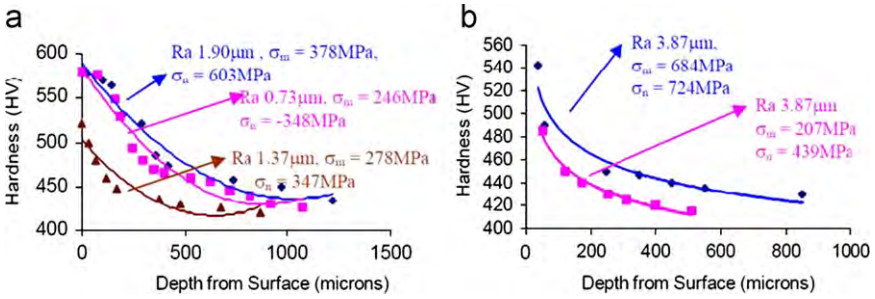

Fig. 19. The hardness profile of milled UDIMET 720 at V=11–56 m/min, f=0.056–0.1 mm/tooth, and DoC=0.25–0.75 mm [59].

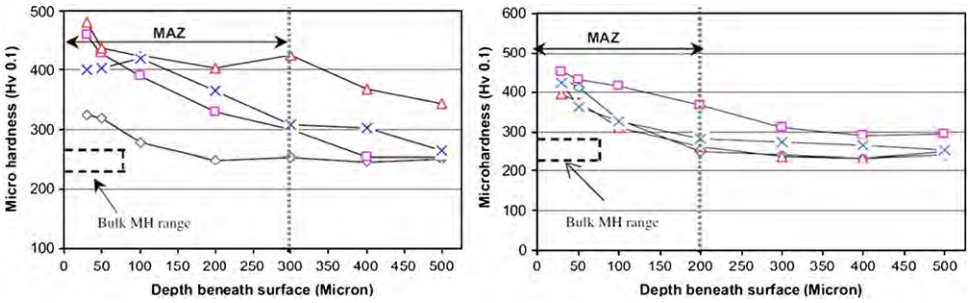

Fig. 20. The hardness profiles of turned IN-718 at V=125–475 m/min, f=0.05–0.15 mm/rev, and DoC=0.5–1 mm [48].

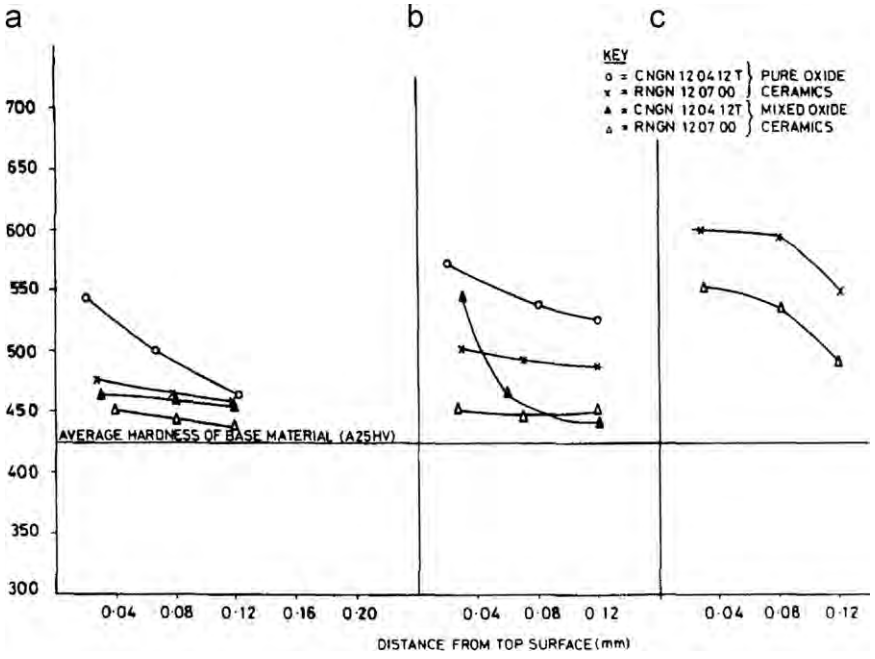

Fig. 21. Hardness dependence for tool wear on turned IN-718 (a) at the start of cutting, (b) after 1 min of cutting, and (c) after 3 min of cutting, at V=152 m/min, f=0.125 mm/rev, and DoC=2 mm [26].

Similar results were found for another titanium-based alloy Ti-6246 elsewhere [15] (Fig. 24). Sun and Guo [10]'s study for Ti-64 is for milling at V=65–110 m/min, f=0.06–0.14 mm/tooth, and DoC=1.5 mm (Fig. 25), and they showed that surface hardness can go up to ~1450 HK (25 g) while the bulk hardness is ~900 HK (25 g).

Experiments on gamma-titanium aluminide for both turning at V=10–25 m/min, f=0.05–0.1 mm/rev, and DoC=0.3–0.7 mm [17] (Fig. 26) and at V=300 m/min, f=0.05 mm, and DoC=0.1 mm [85] (Fig. 27) as well as milling at V=70–120 m/min, f=0.06–0.12 mm/tooth, and DoC=0.1–0.5 mm [18] indicate that the surface of the machined material can become up to 40% harder than the bulk material. Ginting and Nouari [14] examined Ti-6242S alloy in their study and showed that 50 μm deep into the machined surface, the hardness of the material drops to around 320–330 HV_{100} compared to the bulk material hardness of 354 HV_{100}, which is followed by an increased hardness at 200 μm depth into the machined surface to ~370–390 HV_{100}, and hardness value is decreased to bulk material

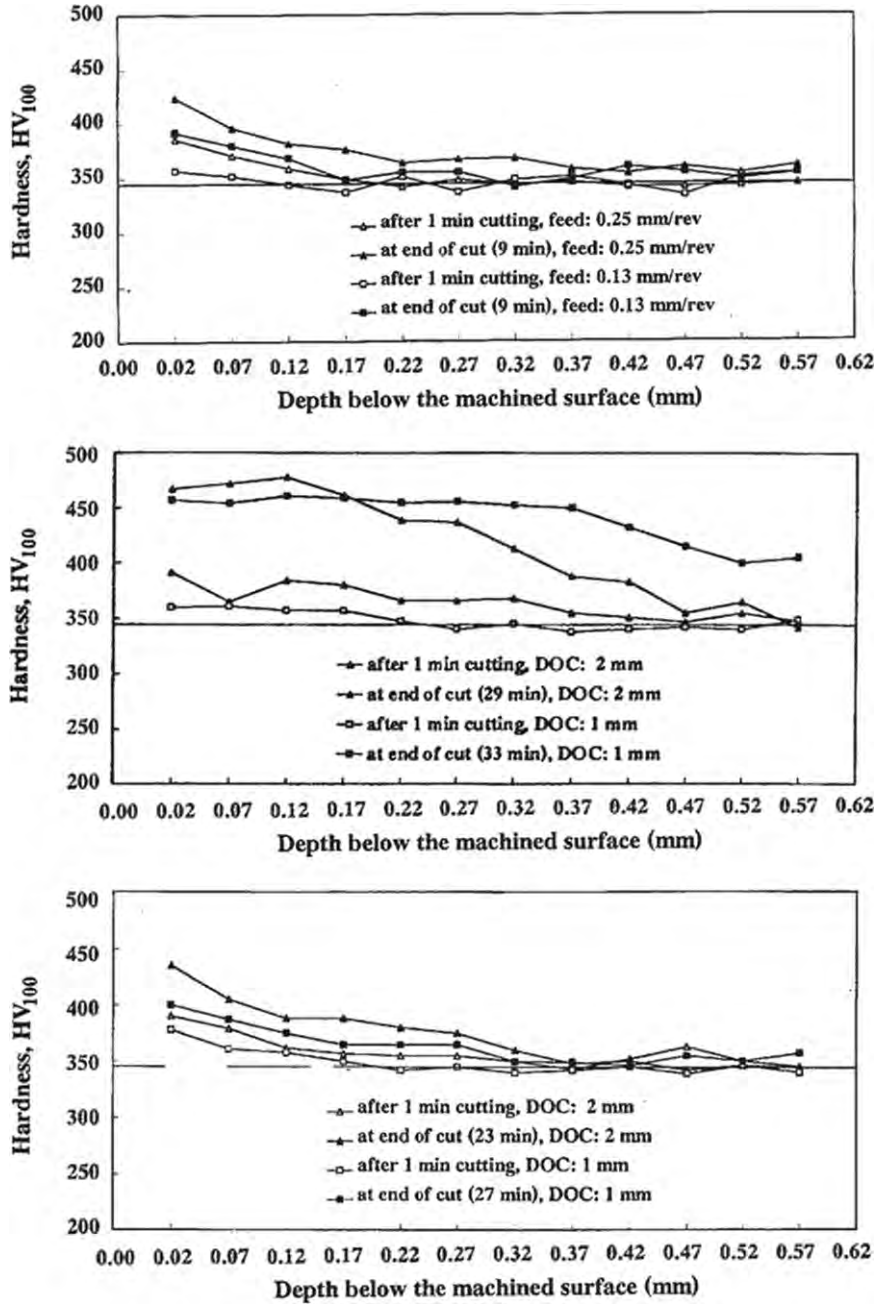

Fig. 22. Microhardness profiles through the depth of the material after turning IN-718 at $V=32$–56 m/min, $f=0.13$–0.25 mm/rev, and $DoC=1$–2 mm [30].

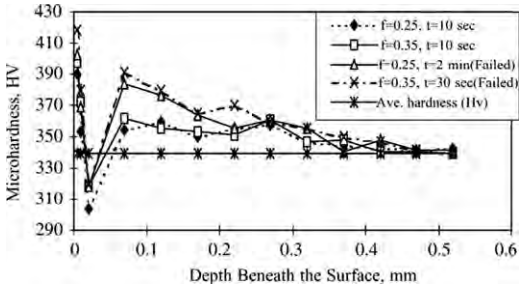

Fig. 23. The hardness profiles of turned Ti-64 at $V=100$ m/min, $f=0.25$–0.35 mm/rev, and $DoC=2$ mm [6].

level at ~300–350 μm deep into the machined surface (Figs. 28 and 29). They studied this pattern for dry milling of Ti-6242S under $V=100$–125 m/min, $f=0.15$–0.2 mm/tooth, $DoC=2$ mm for both uncoated carbide tools (Fig. 28) and multi-layer CVD-coated carbide tools (Fig. 29). However, their measurements do not show any depth level below 50 μm, which is the estimated location of most severe work hardening. They believe that the thermal softening effect up to 100 μm depth is greater than the work-hardening effect, which is the reason for lower hardness values, and after that depth, the thermal softening effect becomes lower than work-hardening effect, which is the main reason for the higher hardness values [14]. They show that the recrystallization structure at those depths into the machined surface also support the conjecture that hardening of the material is directly related to grain sizes. Their findings indicate that when the operating conditions are at their lightest ($V=100$ m/min, $f=0.15$ mm/tooth), the peak values for both low hardness and high hardness locations are closer to the bulk material hardness, whereas the most severe machining conditions ($V=125$ m/min, $f=0.2$ mm/tooth) show the most diversion from the bulk material hardness value at the peak points. While machining shape memory alloys based on NiTi

(α-NiTi), researchers found similar patterns of increased hardness at the surface at V=5–160 m/min, f=0.05–0.2 mm/rev, and DoC=5 mm (Fig. 30) [65].

These studies show that both turning and milling processes can create a harder level on the surface of the machined material, which can lead to a work hardening layer or a white layer to form. Both titanium-based and nickel-based materials exhibit similar patterns of higher hardness on the surface.

3.4. Surface roughness

There are many methods to quantify the surface integrity of a part, and the most widely used method is the surface roughness. It is considered to be the primary indicator of the quality of the surface finish, and reported by many scholars. In titanium and nickel alloys, traditional machining processes have been insufficient to generate surface roughness values low enough to suffice for the end product, so generally post-processing techniques such as laser shock peening or ball burnishing are used.

The temperatures created during high-speed machining (end-milling and turning) of IN-718 and titanium alloy 6Al–6V–2Sn were found to play a major role in tool wear, which is a significant factor in surface roughness of materials [1,20]. The built-up layer that is formed on the tool flank face can push the tool off from its original route to increase the roughness [18], and the cutting parameters

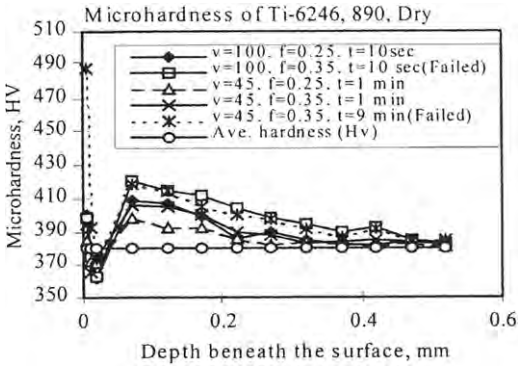

Fig. 24. The hardness profile of turned Ti-6246 at V=45–100 m/min, f=0.25–0.35 mm/rev, DoC=2 mm [15].

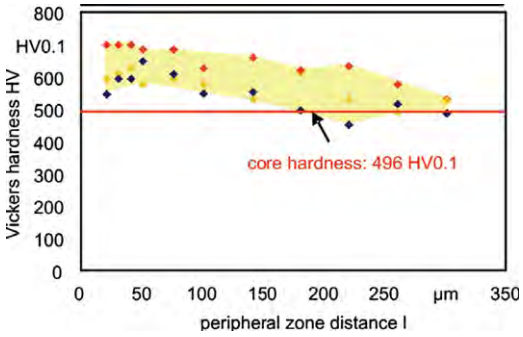

Fig. 27. Microhardness profile of γ-TiAl when turning under V=300 m/min, f=0.05 mm, DoC=0.1 mm [85].

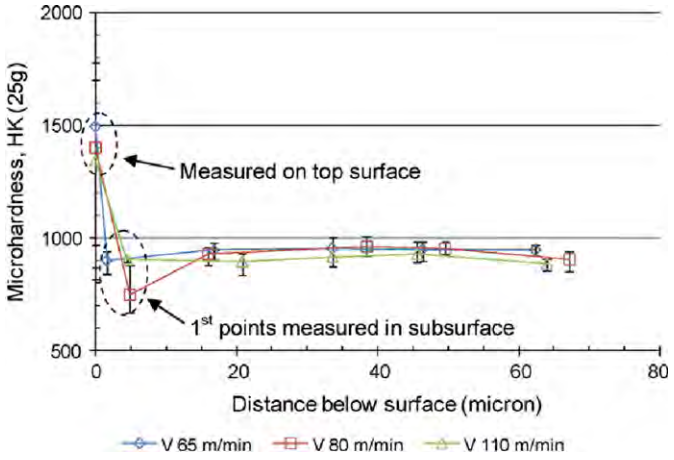

Fig. 25. Microhardness profile of milled Ti-64 at V=65–110 m/min, f=0.06–0.14 mm/tooth, and DoC=1.5 mm [10].

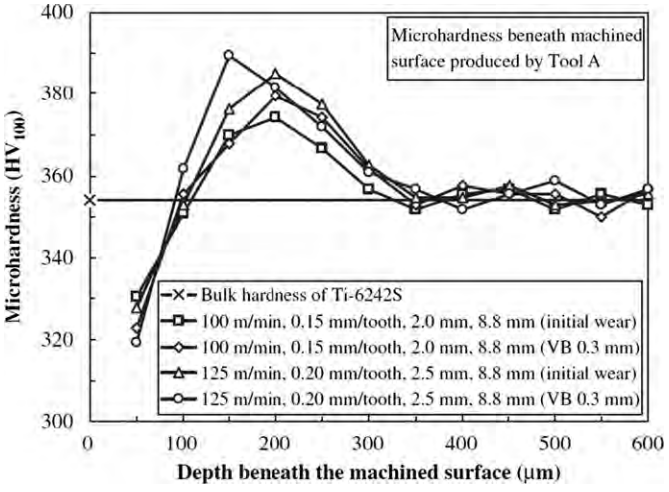

Fig. 28. Microhardness profiles for dry milling Ti-6242S under V=100–125 m/min, f=0.15–0.2 mm/tooth, DoC=2 mm with uncoated carbide tool [14].

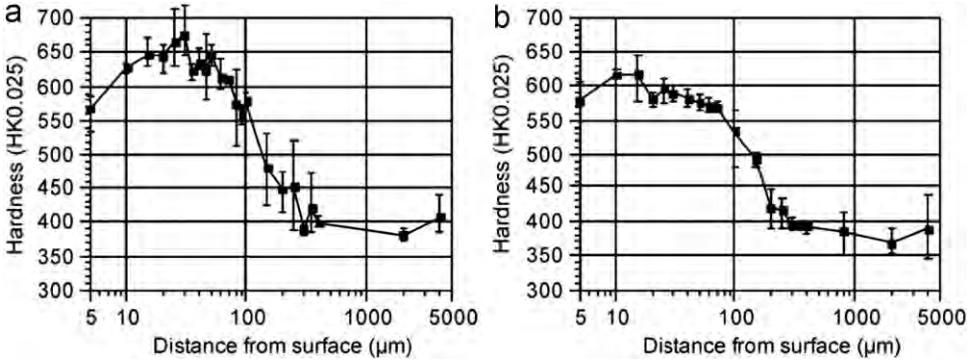

Fig. 26. Microhardness profile of gamma-titanium aluminide after milling at V=70–120 m/min, f=0.06–0.12 mm/tooth, and DoC=0.1–0.5 mm [17].

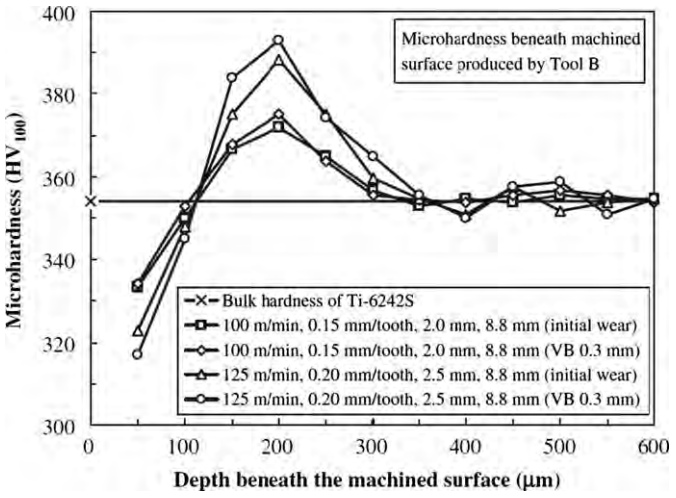

Fig. 29. Microhardness profiles for dry milling Ti-6242S under V=100–125 m/min, f=0.15–0.2 mm/tooth, DoC=2 mm with a multi-layer CVD-coated alloyed carbide tool [14].

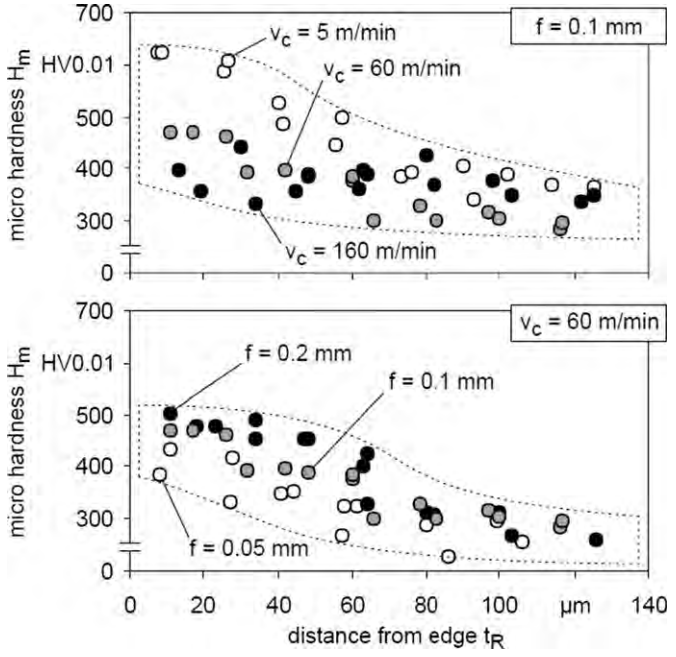

Fig. 30. Microhardness profile of α-NiTi when drilling under V=5, 60, 160 m/min, f=0.05, 0.1, 0.2 mm, and DoC=5 mm [65].

are also very effective on the changes in surface roughness [59]. The researchers have reported that cutting speed [1,6,14,10,15], feed rate [1,10,31] and depth of cut [10,31] are effective to some degree in increasing surface roughness, but mainly with increasing cutting speed, surface roughness increases for both Ti-6246 [15] and Ti-64 [6,8,10]. Also, the tool parameters such as tool insert shape, the cutting edge parameters, insert rake type, the nose radius, and the coolant selection also affect the surface roughness values [35]. According to this study, round inserts create better surface finish due to their longer contact length than square inserts, and honed edges also create better surfaces because of their rounded edge preventing the tool insert from excessive chipping [35]. Positive rakes, bigger nose radii, and use of coolant also improved the surface finish in turning age hardened IN-718 with coated carbide tools at V=60 m/min, f=0.1 mm/rev, and DoC=0.5 mm [35]. Coelho et al. [36] reported that surface roughness values below 500 nm was possible to achieve if IN-718 is turned at V=500 m/min, f=0.1 mm/rev, and DoC=0.35 mm, by using a modified tool edge of round-shaped PCBN and Ceramic tools, while the tool wear is expected to be very rapid under these conditions.

When the tool is fresh, the surface roughness values are found to be higher than with slightly used tools, and the tool wear close to its half-life resulted in slightly decreased surface roughness values than its fresher times. This effect can be considered as the 'warming up' of the tool material, because when the tool is first used, there can be micron-level sharp edges or peaks at its surface that can be trimmed out to create a smoother, or at least a better fit contact surface with the workpiece. When approaching its half-life, the tool is more fit to the workpiece that the surface roughness values decrease. However, after the half-life, the tool starts wearing even more, and this causes anomalies in the tool-workpiece contact surface, which increases the surface roughness values significantly [6,15].

According to the researchers, the surface roughness values while turning Ti-64 at f=0.35 mm/rev and DoC=2 mm at tool life increases when the cutting speed is increased from 45 to 100 m/min gradually [6,15] (Fig. 31). Same material showed similar behavior when milled at V=40–160 m/min, f=0.1 mm/tooth, and DoC=1 mm as well [8]. Their results were for uncoated carbide and PCD tools and the two tool options resulted similarly in terms of surface roughness, while PCD tools were found to be slightly more advantageous (Fig. 32). Feed rate was declared to be the most dominant parameter to affect the surface roughness in machining IN-718 at V=32,125 m/min, f=0.075–0.6 mm/rev, and DoC=0.5,2 mm, and as feed increased, surface quality lowered [31]. Also, turning of IN-718 at V=32–56 m/min, f=0.13–0.25 mm/rev, and DoC=1–2 mm agreed that increasing the feed from 0.13 to 0.25 mm/rev results in significant deterioration of surface, leading to higher surface roughness measurements [30]. Joshi et al. [59] comment in the same direction for another nickel-based alloy UDIMET 720 after milling at V=11, 56 m/min, f=0.056–0.1 mm/tooth, and DoC=0.25 mm that increasing the feed rate made the surface rougher. Ginting and Nouari [14] agree furthermore for milling a titanium-based alloy Ti-6242S that increasing feed from 0.15 to 0.2 mm/tooth at V=100–125, DoC=2–2.5 mm increases surface roughness. Also, some researchers found that for some materials and conditions when the depth of cut was increased, surface quality lowered again [31], whereas other researchers disagreed by showing that for other materials and cutting conditions, depth of cut does not have a significant effect on surface roughness [14].

These effects are reported to be due to thermal and mechanical cycling, microstructural transformations, and mechanical and thermal deformations during machining processes [86]. The effects

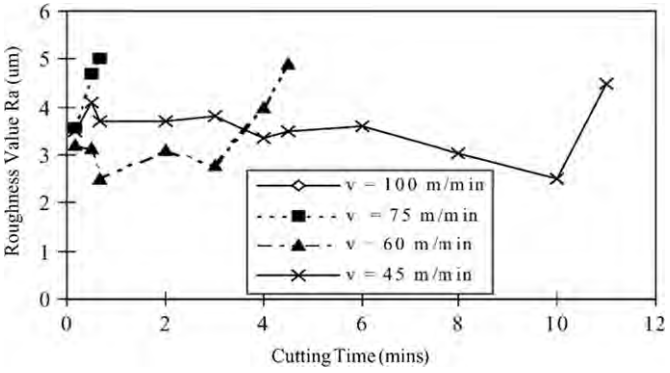

Fig. 31. Surface roughness values when turning Ti-64 with V=45–100 m/min, f=0.35 mm/rev, and DoC=2 mm [6,15].

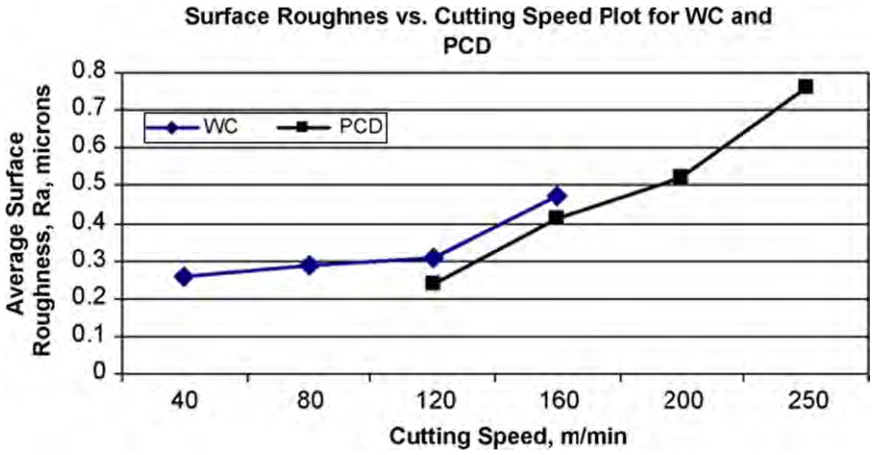

Fig. 32. Average surface roughness values for changing cutting speed for Ti-64 at V=40–160 m/min, f=0.1 mm/tooth, DoC=1 mm [8].

of parameters can vary from material to material. According to Yang and Liu [72], the integrity of surface can be investigated under a few separate topics that are interrelated, such as the residual stresses, metallurgical alterations, and alterations to mechanical properties of the workpiece material. All of these effects will be effective on the roughness of the surface of the end product, so they need to be included in the analysis of the process.

In a general sense, it has been found by many researchers in different areas and for many different materials and cutting conditions that cutting speed and feed parameters adversely affect the surface roughness. However, when the process material removal rate decreases by either decreasing the feed rate or the cutting speed, or both, the surface quality of the part was observed to be better, and the surface roughness values decreased.

3.5. Residual stresses

After machining processes, the workpiece material is released of the thermomechanical load on top of it due to the machining, but not all of the energy can be retrieved. Some of it is spent to plastic deformation, which causes the material to exhibit some stresses, especially at its free ends: the surface. These stresses that remain in the material after the loading is removed are called residual stresses [4]. They are considered to be due to mainly tensile plastic deformation in the sub-surface of the workpiece material and thermal effects at the surface due to cutting and tool conditions [38,87]. These residual stresses present potential risk in terms of crack initiation, propagation and fatigue failure of end products, and it is necessary to remove tensile surface residual stresses or prevent them from occurring during machining processes. There are many researchers working on the methods of prediction and prevention of residual stresses.

The residual stresses are hard to measure, and it is also hard to model this phenomenon, which creates diversity in the results found in the literature. Many researchers claim that surface residual stresses are tensile [34,35,40,43,88–90]; while some claim they are compressive [18,91–92]. The existence and degree of compressive peak residual stresses are also not agreed upon [40,86,89,91], as well as the depth where residual stresses are leveled [18,40,86]. The effects of cutting parameters and tool parameters [86,88,93–97] are also argued, and different results can be found in the literature.

These different results can be due to different workpiece materials and cutting conditions used as well as the differences in tool parameters. As these studies conclude, residual stress is a very important issue to deal within machining steel, titanium and nickel workpieces. It is mostly found that residual stresses are more tensile at the surface of the workpiece and it becomes compressive as the depth of the workpiece increases to around 50 μm. Then, after approximately 300 μm, the residual stresses diminish. The layer that exhibits tensile residual stresses can be related to white layer formation and the compressive residual stresses after 50 μm can be related to dark layer formation, but further study is needed to explore this possibility. It is the general observance that an increase in feed rate makes the residual stresses more tensile at the surface, as shown in Figs. 33 and 34 [10,40,48] and more compressive in the peak compressive depth, especially at higher cutting speeds [16], where the peak residual stresses might become less compressive with increasing feed in lower cutting speeds [16]. Outeiro et al. [47] found that if coated tools were used, the surface residual stresses became less tensile, while the peak compressive residual stresses increased in the compressive direction, as well as occurring at a deeper level (Fig. 35).

Also, some researchers have found for both turning nickel alloy IN-718 at V=40 m/min, f=0.15–0.25 mm/rev, DoC=0.25 mm [40], and at V=125–475 m/min, f=0.05–0.15 mm/rev, and DoC=0.5–1 mm [48] and milling titanium alloy Ti-834 at V=11–56 m/min, f=0.056–0.1 mm/tooth, DoC=0.25–2 mm [16] that with increasing cutting speed, tensile residual stresses tend to become more compressive. Sun and Guo [10] also claim for milling Ti-64 at V=50–110 m/min, f=0.08–0.14 mm/tooth, DoC=2 mm that with increasing cutting speed, surface residual stresses became more compressive. However, findings of Schlauer et al. [33] (Fig. 36), Sadat [24] (Fig. 37), Sadat et al. [25] (Fig. 38) for turning, Arunachalam et al. [35] (Fig. 39) for facing, Derrien and Vigneau [28] and Guerville and Vigneau [37] for dry milling (Fig. 40) and point milling (Fig. 41) IN-718 under various different conditions suggest that the surface residual stresses are more tensile with increasing speed. Moreover, Mantle and Aspinwall [18]found that compressive stresses decreased when the cutting speed was increased in milling gamma-titanium aluminide at V=70–120 m/min, f=0.06–0.12 mm/tooth, DoC=0.1–0.5 mm.

On the other hand, increasing depth of cut is said to decrease compressive residual stresses in milling titanium alloy Ti-834 at V=11–56 m/min, f=0.056–0.1 mm/tooth, DoC=0.25–2 mm [16] and in facing age-hardened IN-718 at V=150–450 m/min, f=0.15 mm/rev, DoC=0.5 mm [35], while it is said to increase compressive residual stresses in turning IN-718 at V=125–475 m/min, f=0.05–0.15 mm/rev, and DoC=0.5–1 mm [48]. In addition, cutting edge geometry is known to affect the compressive/tensile behavior and the magnitude of residual stresses (Fig. 42), and the additional ploughing due to the honed radius compared to chamfered

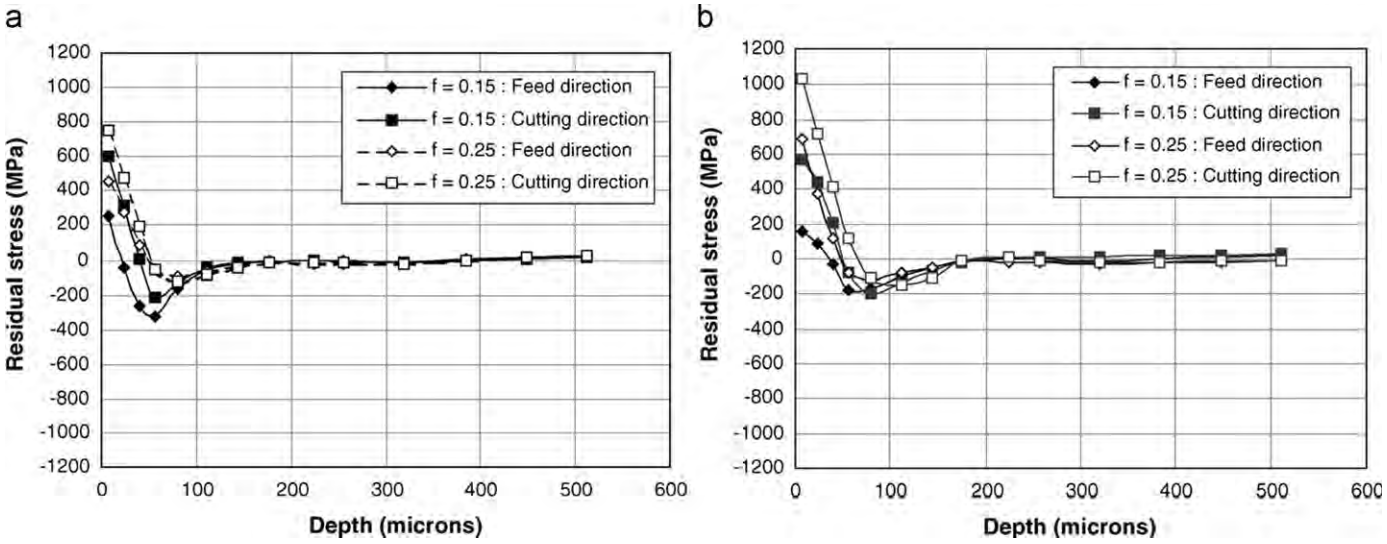

Fig. 33. Residual profiles of (a) new and (b) worn tools while turning IN-718 at V=40 m/min, f=0.15–0.25 mm/rev, DoC=0.25 mm [40].

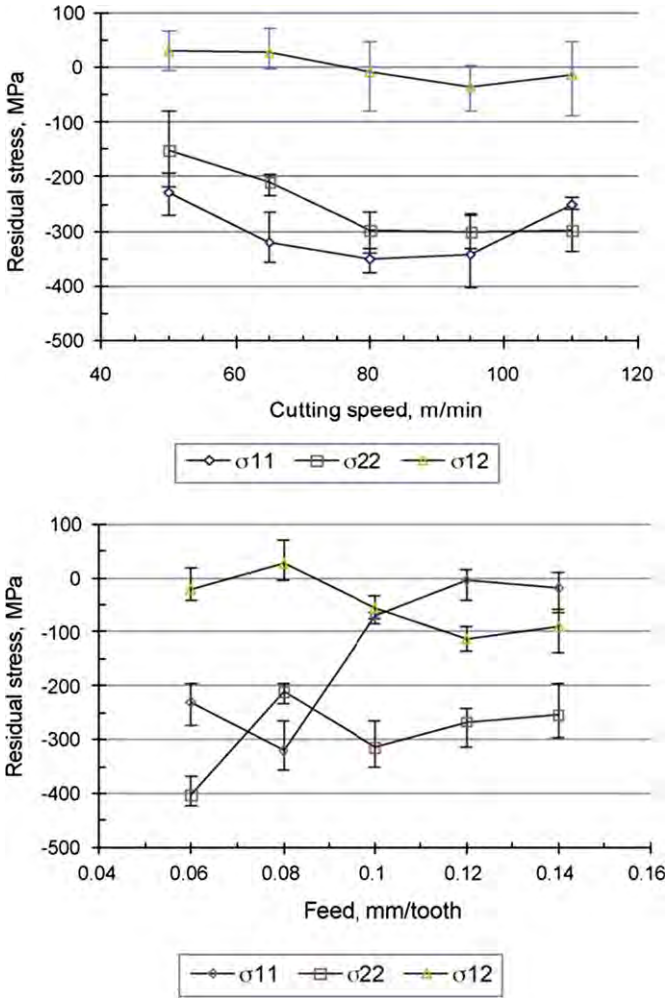

Fig. 34. Residual stress changes with feed rate and cutting speed in end milling of Ti-64 with coated carbide tools at V=50–110 m/min, f=0.06–0.14 mm/tooth, and DoC=1.5 mm [10].

tools is said to increase the compressive nature of residual stresses [48]. The effect of the tool chamfer edge geometry on residual stress is also studied by Coelho et al. [36] for turning IN-718 at

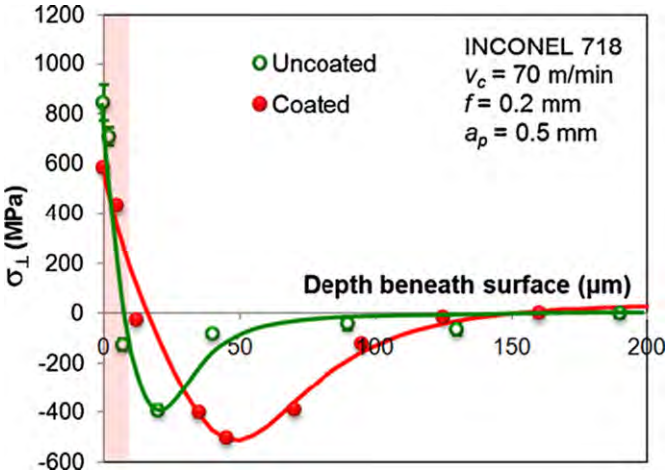

Fig. 35. Residual stress profile of IN-718 after turning at V=70 m/min, f=0.2 mm, and DoC=0.5 mm [47].

V=500m/min, f=0.1 mm/rev, DoC=0.35 mm, where the tool cutting edge preparation was modified and it has been shown to slightly change the measured residual stresses (Fig. 43).

It is also known that with increasing tool wear, tensile residual stresses in the surface of IN-718 during turning increase at V= 40–120 m/min, f=0.15–0.25 mm/rev, DoC=0.25 mm [40], and at V=40–80 m/min, f=0.35 mm/rev, DoC=0.25 mm [41]. This is considered to be happening mainly due to the increase in plastic deformation as well as the rubbing effect causing a friction induced temperature rise. Fig. 44 also shows another study for turning Ti-64 at V=320 m/min, f=0.1 mm/rev, DoC=1 mm , which suggests that as the flank wear increases, the surface residual stresses become more tensile due to increased temperature, the peak compressive residual stresses become slightly less compressive, and the residual stresses deep into the material become tensile rather than compressive as well [5]. Fig. 45 shows the study of Aspinwall et al. [44] for milling IN-718, and they showed that when tool wears, surface residual stresses tend to become tensile, while the peak compressive residual stresses do not change consistently. However, the affected layer of the material has become much deeper with increasing tool wear. Fig. 46 is from the same study of Aspinwall

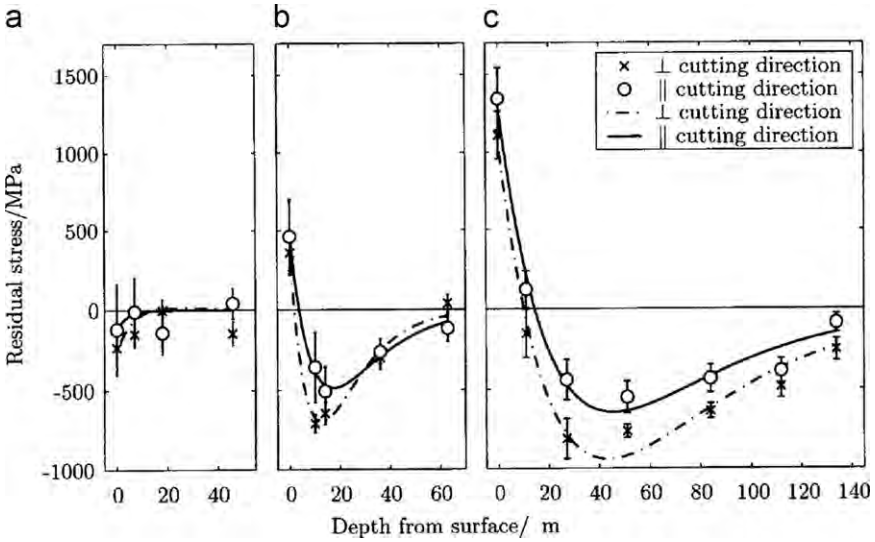

Fig. 36. Residual stress profile after turning IN-718 at f=0.06 mm/rev and (a) 10 m/min, (b) 410 m/min, (c) 810 m/min cutting speed (depth of cut not specified) [33].

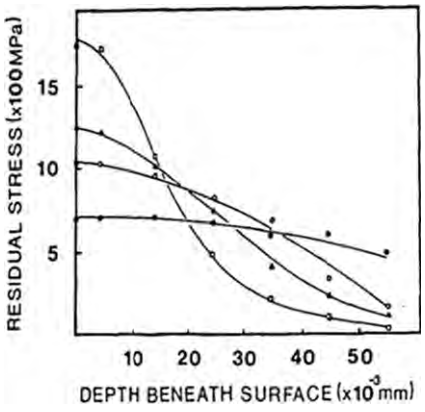

Fig. 37. Residual stress profile of IN-718 after turning at V=0.11–1 m/s, and f=0.11 mm/rev (depth of cut not specified) [24].

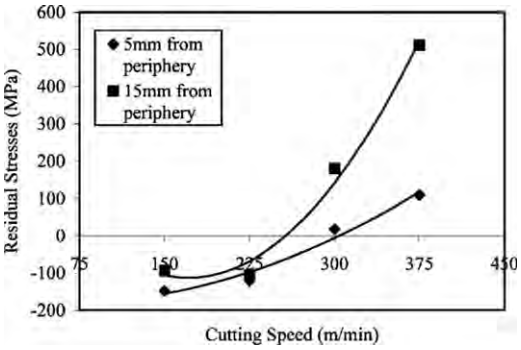

Fig. 39. Change of residual stresses with cutting speed for facing IN-718 at V=150–375 m/min, f=0.15 mm/rev, DoC=0.5 mm [35]

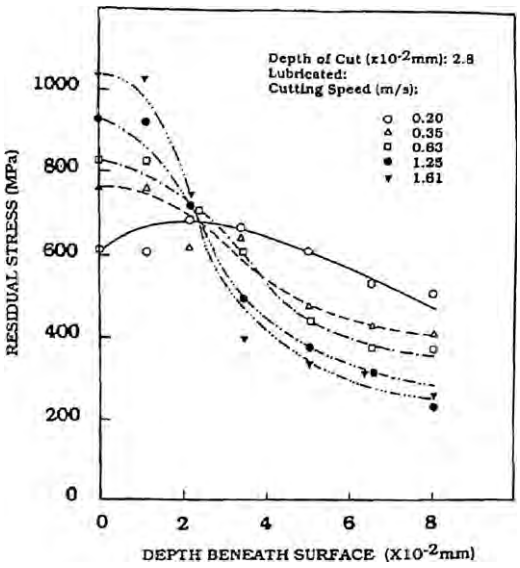

Fig. 38. Residual stress profile of IN-718 after turning at V=0.2–1.61 m/s, and DoC=0.028 mm (feed rate not specified) [25].

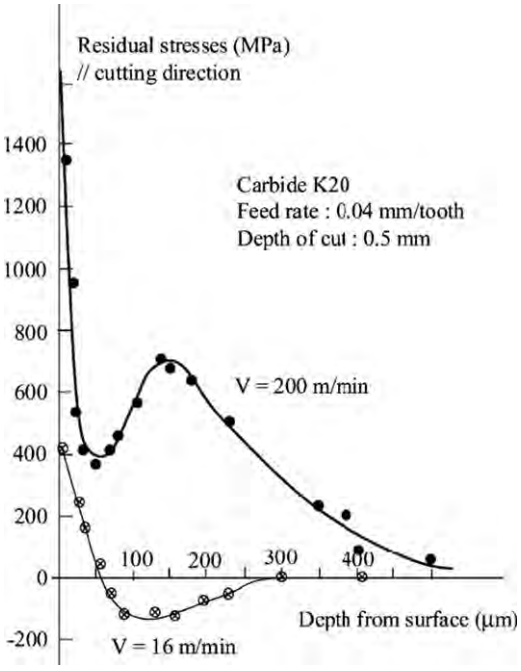

Fig. 40. Residual stress profile of IN-718 after dry milling at V=16–200 m/min, f=0.04 mm/tooth, and DoC=0.5 mm [28,37,38].

et al. [44], where they show the effect of cutter orientation and workpiece tilt angle as well as tool wear on the residual stresses, and they depicted that by changing the cutter orientation or the workpiece tilt angle, without changing the working parameters, it is possible to change the residual stresses from tensile to compressive, or alter the magnitude of the residual stresses.

As the tool starts from its fresh state, there might be some time needed for it to adjust its contact points according to the machining process and the workpiece, so relatively higher surface roughness and tensile surface residual stresses can be observed. However, after the initial warming up period at the fresh start, and especially after its predefined half-life, the tool wear becomes an important aspect of the surface quality, and residual stresses become more tensile at the surface and white layers become more visible as well, owing to the increasing plastic deformation and temperature gradients during machining.

3.6. Summary of surface integrity findings and trends

All of the work reviewed in this paper is summarized in Figs. 47, 48 and 49 together with remarks about this specific work in Table 2, 3 and 4 respectively. The major findings from work reviewed are given as trends in those figures.

The researchers have reported that increasing the cutting speed created higher hardness values as shown in Fig. 47 while increasing the feed rate had a minimal effect on the microhardness profile on the machined surface as shown in Fig. 48.

The researchers also reported that cutting speed, feed rate and depth of cut are effective to some degree in increasing surface roughness as depicted in Figs. 47 and 49, respectively. But mainly with increasing cutting speed, surface roughness increases as shown in Fig. 47.

Feed rate was declared to be the most dominant parameter to affect the surface roughness in machining IN-718 and as feed increased, surface quality lowered (Fig. 48).

Also, some researchers found that for some materials and conditions when the depth of cut was increased, surface quality lowered again (see Fig. 49), whereas other researchers disagreed by showing that for other materials and cutting conditions, depth of cut does not have a significant effect on surface roughness.

It is the general observance that increases in depth of cut and feed rate have some effect on making the residual stresses more

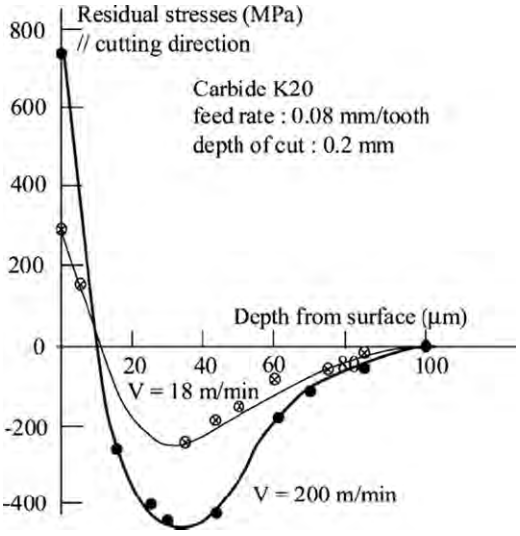

Fig. 41. Residual stress profile of IN-718 after point milling at V=18–200 m/min, f=0.08 mm/tooth, and DoC=0.2 mm [28,37,38].

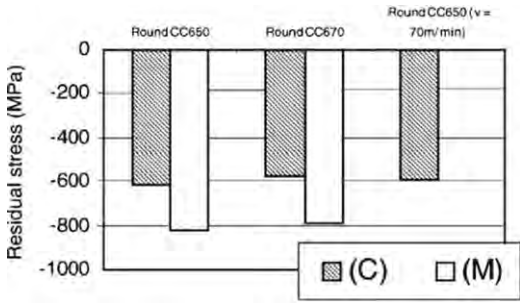

Fig. 43. Residual stresses after turning IN-718 at V=70–500 m/min, f=0.1 mm/rev, and DoC=0.35 mm with different edge preparation chamfered cutting tools (C: commercial chamfer, M: modified chamfer) [36].

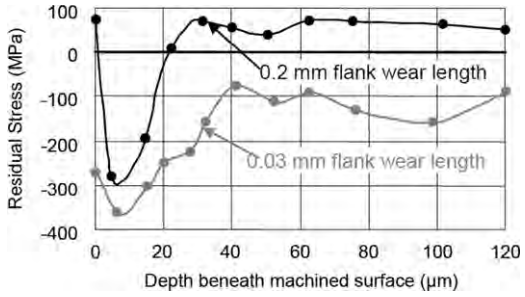

Fig. 44. Effect of flank wear on residual stresses after turning Ti-64 at V=320 m/min, f=0.1 mm/rev, DoC=1 mm [5].

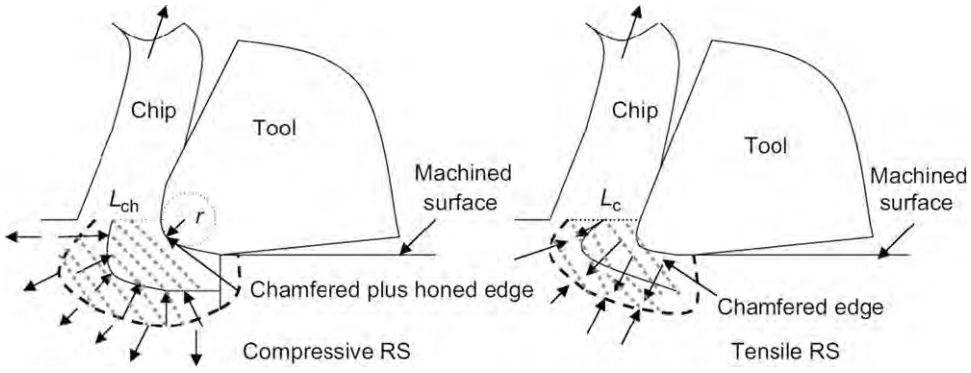

Fig. 42. Illustration for the effect of tool geometry on residual stresses in machining IN-718 [48].

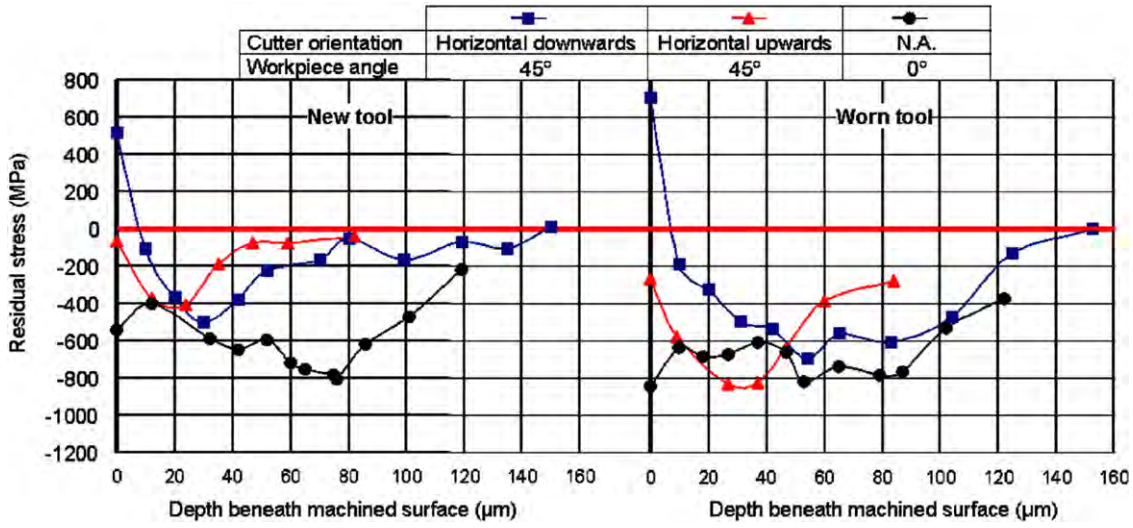

Fig. 45. Residual stress profile after ball end milling IN-718 at V=90 m/min, f=0.2 mm/tooth, and DoC=0.5 mm [44].

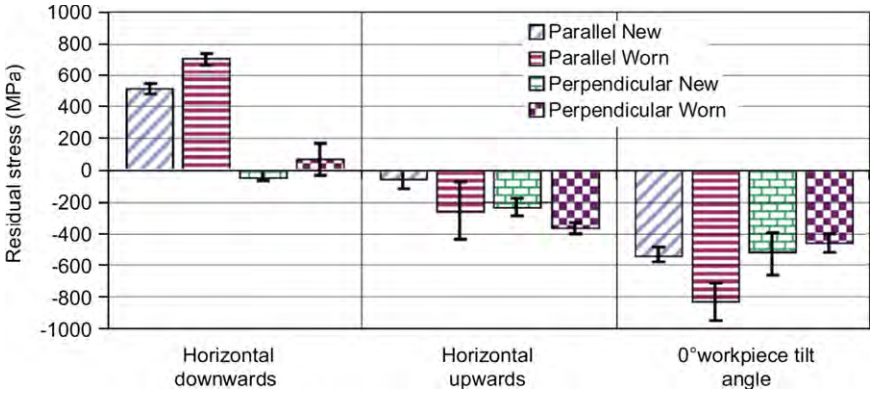

Fig. 46. Change of residual stresses with cutter orientation/workpiece tilt angle, and between new and worn tools for IN-718 at V=90 m/min, f=0.2 mm/tooth, and DoC=0.5 mm [44].

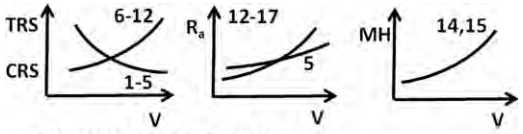

1: IN-718 (Sharman et al. 2004)
2: IN-718 (Sharman et al. 2006)
3: Ti-834 (Sridhar et al. 2003)
4: IN-718 (Pawade et al. 2008)
5: Ti-64 (Sun&Guo 2009)
6: IN-718 (Sadat 1987)
7: IN-718 (Sadat et al. 1991)
8: IN-718 (Derrien&Vigneau 1997)
9: γ-TiAl (Mantle&Aspinwall 2001)
10: IN-718 (Guerville&Vigneau 2002)
11: IN-718 (Schlauer et al. 2002)
12: IN-718 (Arunachalam et al. 2004b)
13: Ti-4.5Al-4.5Mn (Zoya&Krishnamurthy 2000)
14: Ti-6246 (Che-Haron 2001)
15: Ti-64 (Che-Haron&Jawaid 2005)
16: Ti-64 (Nurul-Amin et al. 2007)
17: Ti-6242S (Ginting&Nouari 2009)

Fig. 47. Effects of cutting speed (V) on surface quality measures (see Table 2 for reference information).

tensile at the surface and more compressive in the peak compressive depth, especially at higher cutting speeds , where the peak residual stresses might become less compressive with increasing feed in lower cutting speeds as shown in Fig. 48. Also, some researchers have found for both nickel alloy IN-718 and titanium alloy IMI-834 that with increasing cutting speed, tensile residual stresses tend to become more compressive (Fig. 47).

4. Methods of analysis and investigation of machining-induced surface integrity

4.1. Experimental surface integrity analysis

There have been many scholars conducting experiments in order to measure different means of surface integrity such as surface roughness, microhardness, and residual stresses, and their outcomes have been very useful for analytical or FEM-based analysis methods of analysis as well. These experiments may not provide answers on their own, but it is not always possible to outline the effect of every possible case via experimentation, or it is too expensive and time-consuming to do so. However, the outcomes of these experiments can be used in order to validate and compare the findings via analytical or FEM-based predictions. They can also be useful in order to constitute the basis of the experimental modeling and empirical studies, since these studies are based on the exact data in order to find the relationship coefficients between the input and the output parameters.

The surface integrity analysis techniques are generally dedicated to analyzing the surface of the workpiece in order to find out

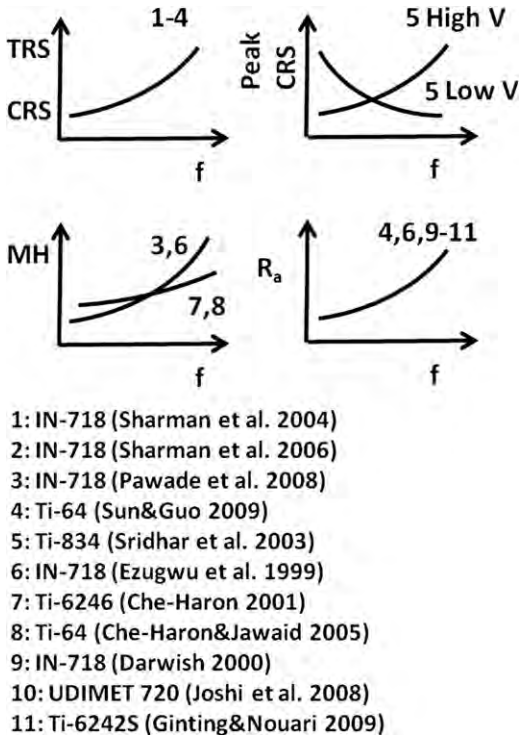

Fig. 48. Effect of feed rate (f) on surface quality measures (see Table 3 for reference information).

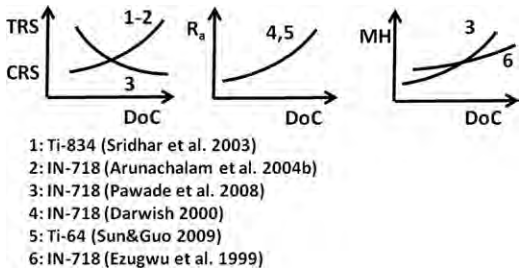

Fig. 49. Effect of depth of cut (DoC) on surface quality measures (see Table 4 for reference information).

the structure of the end product, utilizing tools such as profilometers and optical microscopes. These devices can provide information about the topological structure of the surface, which forms the basis to understand the outcomes of the experiments.

Optical microscopes are used to acquire the images of the micro-specimen. The digitized image is then manipulated through threshold adjustments in order to differentiate between the white and dark layers as well as the bulk material [11,14,78]. This eliminates the gradual changes between layers, but enables observers to differentiate between the layers and calculate the layer depths.

Surface profilometer, white-light interferometry, and other techniques are also used to achieve 3-D images of the surface after machining [14]. Vickers method microhardness measurement is often used in order to obtain sub-surface alterations to the workpiece material, and microstructural etching by a fluid reagent in order to measure the microstructural alterations.

These experimental studies also focused on the residual stresses and white layer formations on the workpiece material. The residual stresses are measured to instigate from tensile region, become compressive after a depth called the tensile layer, and then level out at around 200–400 μm depth into the workpiece [93]. Sometimes, they do not undergo a transition from tensile to compressive, though, and it can be observed that the residual stresses start from tensile and level out as tensile stresses [75]. These measurements of residual stress are often done by utilizing X-ray diffraction and electropolishing techniques [87,96], and residual stresses can be observed even in the absence of phase transformations and microstructural alterations, which separates it from white layer formation. X-ray diffraction is a non-destructive analytical measurement technique used to investigate the crystalline structure, grain size and orientation, and strain of materials using an X-ray beam. On the other hand, electropolishing is a method to remove surface material from metallic surfaces and polishing the surface without altering the residual stresses at any level, so that sub-surface residual stress measurement can be done without inaccuracies caused by post-machining.

Three different methods can be used in order to understand the white layer formation in the machined surfaces: scanning electron microscopy [74,75,82,98,99], X-ray diffraction [79,80], and Mössbauer Spectrometry [79]. Using these techniques, researchers found out that there are austenitic and martensitic structures within the surface white layer, which shows that phase transformations happen during the formation of white layers [79]. X-ray diffraction method is also used for residual stress measurements.

Axinte et al. [43] have studied the surface integrity of nickel-based alloys obtained via powder metallurgy means. They utilized rough and finish turning operations on nickel-based alloy workpieces and examined the results for surface integrity and residual stresses. They found out that the adhesive characteristic of the material results in redeposition of the workpiece material after it is machined to create a much rougher surface than it should have been (Fig. 50). They resulted from these experiments that varying depth of cut values in successive passes for this type of new technology material is the optimum solution to the machinability problem, since these differences in depths of cut prevents redeposition of workpiece material onto the workpiece itself to some extent.

The experimental results show that it is very hard to measure the residual stresses, which can be observed from the fact that the results differ between the findings of researchers. The general idea is that there are some tensile residual stresses or very low compressive residual stresses at the surface of the machined workpiece, which become compressive after some depth, and make a peak at a depth that can be classified as the 'peak depth' or 'tensile layer depth', and then level after some depth through the bulk material. Experimental studies on white layer formation are more decisive on the knowledge that increases in cutting speed result in decreasing white layer thicknesses.

4.2. Experimental modeling and empirical techniques

Many researchers try to find empirical relationships between the input and output parameters directly by using experimental results, since analytical solutions are often difficult to formulate, and FEM-based solutions might take time. Especially residual stresses and surface roughness values are experimented for a few cutting conditions, then empirical equations are found out using the result of these experiments with the input parameters being a combination of cutting speed, feed, depth of cut, tool properties and workpiece properties most of the time. These studies are not based on analytical realizations, but they provide a good knowledge about the possible outcomes of similar cutting conditions with similar tool and workpiece materials.

Most researchers have utilized empirical solutions in order to predict the residual stresses [16,87,95,100], surface roughness [86], and white layer thickness [99], as well as the yield strength of and plastic strain on the workpiece material [48]. The effects of cutting

Table 2
Material, process, and parameter information for Fig. 47.

Reference	Work material	Tool material	Process	Parameters	Remarks
Sadat [24]	IN-718	Carbide $\gamma=10^\circ$	Turning	$V=0.11$–1 m/s $f=0.11$ mm/rev	Peak tensile residual stresses increased with increasing cutting speed
Sadat et al. [25]	IN-718	Ceramic $\gamma=5^\circ$	Turning	$V=0.2$–1.61 m/s $DoC=0.028$ mm	Peak tensile residual stresses increased with increasing cutting speed
Derrien and Vigneau [28]	IN-718	Uncoated carbide	Dry milling	$V=16{,}200$ m/min $f=0.04$ mm/tooth $DoC=0.5$ mm	Increasing the cutting speed from 16 to 200 m/min increased immediate sub-surface tensile residual stress from 400 to 1400 MPa, and eliminated the 100 μm depth peak compressive residual stress
Zoya and Krishnamurthy [19]	Ti–4.5Al–4.5Mn	PCBN	Turning	$V=150$–350 m/min $f=0.05$ mm/rev $DoC=0.5$ mm	Increasing the cutting speed from 150 to 350 m/min increased surface roughness from 0.3 to 0.4 μm
Che-Haron [15]	Ti–6Al–2Sn–4Zr–6Mo (380 HBS)	Uncoated carbide (1760 HNV) $\gamma=-6^\circ$	Turning	$V=45$–100 m/min $f=0.25$–0.35 mm/rev $DoC=2$ mm	Due to increasing tool wear, when cutting speed is increased, surface roughness increases as well. Also, higher microhardness values were recorded for higher cutting speed
Mantle and Aspinwall [18]	γ-TiAl	Uncoated carbide	Milling	$V=70$–120 m/min $f=0.06$–0.12 mm/rev $DoC=0.2$–0.5 mm	Increasing the cutting speed decreased the amount of compressive residual stresses observed
Schlauer [33]	IN-718 (annealed and aged)	Uncoated carbide, 20° chamfered	Turning	$V=10{,}410{,}810$ m/min $f=0.01{,}0.06{,}0.11$ mm	Increasing cutting speed from 10 to 410 and 810 m/min changed compressive surface residual stresses to tensile, as well as increasing peak compressive residual stresses
Guerville and Vigneau [37]	IN-718	Uncoated carbide	Point milling	$V=18{,}200$ m/min $f=0.08$ mm/tooth $DoC=0.2$ mm	Increasing the cutting speed from 18 to 200 increased surface tensile residual stress from 250 to 750 MPa, and the peak compressive residual stress from 200 to 450 MPa
Sridhar et al. [16]	Ti-IMI 834	Coated carbide (TiN)	Milling	$V=11.56$ m/min $f=0.056{,}0.1$ mm/tooth $DoC=0.25{,}2$ mm	When the cutting speed was increased from 11 to 56 m/min, the peak residual stresses decreased at low f and DoC, but increased at high f and DoC
Arunachalam et al. [35]	IN-718 (36 HRC)	CBN and mixed ceramic	Facing	$V=150$–450 m/min $f=0.15$ mm/rev $DoC=0.05$–0.5 mm	Increase in cutting speed changed residual stresses from compressive (-100MPa) to tensile (500MPa), and increased surface roughness
Sharman et al. [1]	IN-718 (38 HRC)	Coated carbide $\gamma=9^\circ$ (TiCN/Al_2O_3/TiN)Uncoated carbide $\gamma=7^\circ$	Turning	$V=40$–120 m/min $f=0.15$–0.25 mm/rev $DoC=0.25$ mm	At the higher cutting speeds, they observed that the maximum tensile residual stress was increased
Che-Haron and Jawaid [6]	Ti-64 (250–300 HBS)	Uncoated carbide (1760 HNV) $\gamma=-6^\circ$	Turning	$V=45$–100 m/min $f=0.25$–0.35 mm/rev $DoC=2$ mm	Due to higher tool wear, increasing cutting speed increases surface roughness. Also, higher microhardness values were recorded for higher cutting speed
Sharman et al. [40]	IN-718	Coated carbide $\gamma=7$–9° (TiCN/Al_2O_3/TiN)	Turning	$V=40$–120 m/min $f=0.15$–0.25 mm/rev $DoC=0.25$ mm	Increasing the cutting speed from 40 to 80 and 120 m/min decreased the surface tensile residual stresses from ~600 to ~200 MPa for the same conditions
Nurul-Amin et al. [8]	Ti-64	Uncoated Carbide and PCD	End milling	$V=40$–160,120–250 m/min $f=0.1$ mm/tooth $DoC=1$ mm	For both uncoated carbide and PCD tools, increasing the cutting speed from 40 to 160 and from 120 to 250, respectively, increased surface roughness
Pawade et al. [48]	IN-718	PCBN	Turning	$V=125{,}300{,}475$ m/min $f=0.05{,}0.1{,}0.15$ mm/rev $DoC=0.5{,}0.75{,}1$ mm	A small increase in tensile residual stresses observed when V increased from 125 to 300 m/min, but a significant change from tensile to compressive residual stresses observed when V increased to 475 m/min
Ginting and Nouari [14]	Ti-6242S	Uncoated and coated carbide (TiN, TiC, TiCN)	Milling	$V=100$–125 m/min $f=0.15$–0.2 mm/tooth $DoC=2$–2.5 mm	Increasing the cutting speed increases the observed surface roughness with uncoated tools, but decreases slightly with coated tools
Sun and Guo [10]	Ti-64	Coated carbide (TiAlN)	End milling	$V=50$–110 m/min $f=0.06$–0.14 mm/tooth $DoC=1.5$ mm	Increasing cutting speed gradually from 50 to 110 m/min in 15 m/min increments increased surface roughness in cutting direction from ~0.6 R_a to ~0.8–0.9 R_a, as well as increasing the compressive residual stresses from ~150 to ~300 MPa

speed, feed rate, tool nose radius, workpiece properties, and depth of cut are mainly investigated, but virtually any affecting factor can be outlined in these types of studies. The results can also be found with analytical predictions, and the predictions that are not in good enough agreement can be approximated to the experimental data using correction coefficients, so that the effects of cutting parameters can be observed more easily [87]. Different approximation techniques such as least squares estimation can be utilized in these models, and although generally first order linear or second-order models are used, any type of equation can be created and the one that gives the best approximation can be chosen. Pawade et al.[48] used cutting conditions in order to predict the yield strength of the material, as

Table 3
Material, process, and parameter information for Fig. 48.

Reference	Work material	Tool material	Process	Parameters	Remarks
Ezugwu et al. [30]	IN-718	Coated carbide (TiN and TiN/TiCN//TiN PVD-coated, TiC/Al_2O_3/TiN CVD-coated)	Turning	V=32–56 m/min f=0.13, 0.25 mm/rev d=1.2 mm	Increasing feed rate from 0.13 to 0.25 mm/rev increases surface roughness significantly, as well as the microhardness at the surface
Darwish [31]	IN-718	Ceramic and CBN	Turning	V=32.125 m/min f=0.075–0.6 mm/rev d=0.5,2 mm	Higher the feed rate, the lower the surface quality
Che-Haron [15]	Ti–6Al–2Sn–4Zr–6Mo (380 HBS)	Uncoated carbide (1760 HNV) $\gamma=-6^\circ$	Turning	V=45–100 m/min f=0.25–0.35 mm/rev DoC=2 mm	Minimal increment in microhardness was observed with increasing feed
Sridhar et al. [16]	Ti-IMI 834	Coated carbide (TiN)	Milling	V=11–56 m/min f=0.056–0.1 mm/tooth d=0.25–2 mm	At low speed (11 m/min), increasing feed reduced sub-surface compressive residual stresses, at high speed (56 m/min), increasing feed increased sub-surface compressive residual stresses
Sharman et al. [1]	IN-718 (38 HRC)	Coated carbide $\gamma=9^\circ$ ($TiCN/Al_2O_3$/TiN) Uncoated carbide $\gamma=7^\circ$	Turning	V=40–120 m/min f=0.15–0.25 mm/rev DoC=0.25 mm	Lower feed rates resulted in lower tensile surface residual stress
Che-Haron and Jawaid [6]	Ti-64 (250–300 HBS)	Uncoated carbide (1760 HNV) $\gamma=-6^\circ$	Turning	V=45–100 m/min f=0.25–0.35 mm/rev DoC=2 mm	Minimal increment in microhardness was observed with increasing feed
Sharman et al. [40]	IN-718	Coated carbide (TiCN/Al_2O_3/TiN) $\gamma=7$–9°	Turning	V=40–120 m/min f=0.15–0.25 mm/rev d=0.25 mm	Lower feed rates resulted in lower tensile surface residual stress
Joshi et al. [59]	UDIMET 720		Milling	V=11,56 m/min f=0.056–0.1 mm/tooth DoC=0.25 mm	Increasing feed rate increases surface roughness
Pawade et al. [48]	IN-718	PCBN	Turning	V=125,300,475 m/min f=0.05,0.1,0.15 mm/rev DoC=0.5,0.75,1 mm	Tensile residual stresses increased with increasing feed, while also increasing microhardness values at the surface
Ginting and Nouari [14]	Ti-6242S	Uncoated and coated carbide (TiN, TiC, TiCN)	Milling	V=100–125 m/min f=0.15–0.2 mm/tooth d=2–2.5 mm	Increasing the feed increases the surface roughness under all cutting conditions
Sun and Guo [10]	Ti-64	Coated carbide (TiAlN)	End milling	V=50–110 m/min f=0.06–0.14 mm/tooth d=1.5 mm	Increasing feed tensile residual stresses at surface increased

well as the strain applied during machining. Sridhar et al.'s [16] findings for titanium-based alloy Ti-834 were based on a linear equation that relate residual stresses (σ) to cutting speed (V), feed (f), and depth of cut (d) as follows:

$$\sigma = b_0 + b_1 v + b_2 f + b_3 d \quad (1)$$

Here, b_i's are coefficients of the equation. Then, they added interactive terms to this equation that enabled them to find similar patterns of residual stress with different models:

$$\sigma = b_0 + b_1 v + b_2 f + b_3 d + b_4 vf + b_5 vd + b_6 fd + b_7 vfd \quad (2)$$

A similar pattern of empirical equation was also utilized by Joshi et al. [59] for nickel-based alloy UDIMET 720, but they found residual stresses in milling direction (σ_m) as well as normal to milling direction (σ_n), surface roughness (R_a), and shear residual stress (τ_{mn}):

$$\begin{aligned}
\sigma_m &= a_1 + a_2 v + a_3 f + a_4 d + a_5 vf + a_6 fd + a_7 vd + a_8 vfd \\
\sigma_n &= b_1 + b_2 v + b_3 f + b_4 d + b_5 vf + b_6 fd + b_7 vd + b_8 vfd \\
R_a &= c_1 + c_2 v + c_3 f + c_4 d + c_5 vf + c_6 fd + c_7 vd + c_8 vfd \\
\tau_{mn} &= d_1 + d_2 v + d_3 f + d_4 d + d_5 vf + d_6 fd + d_7 vd + d_8 vfd
\end{aligned} \quad (3)$$

Here, a_i's, b_i's, c_i's, and d_i's are the coefficients of the empirical equation to be determined. Another similar study was also reported by Subhas et al. [101] for IN-718 where they modeled linear and interactive terms of cutting speed, feed, depth of cut, tool nose radius, and rake angle, and their output variables were circumferential and longitudinal residual stresses, tool life, surface roughness and dimensional instability, summarized in one variable y, where the input parameters are x_i's:

$$y = b_0 + \sum_{i=1}^{5} b_i x_i + \sum_{i=1}^{5} \sum_{j=1}^{5} b_{ij} x_i x_j \quad (4)$$

Pawade et al. [45] also contributed to this type of studies by representing the surface roughness of machined IN-718 in terms of cutting speed, feed rate, and the Young's Modulus of the material, since they found that the depth of cut had a minimal effect, whereas the cutting speed dominated the effect on the surface roughness. The reason to use these different models, though, is because the simplest equations do not fit the data in good accuracy, whereas when the equation involves more complex terms, it becomes closer to experimental findings [99]. Similar equations were observed in studies by researchers investigating the effects of machining steel parts. Axinte and Dewes [86] included the workpiece angle and cutting length in the analysis for milling AISI H13 steel and El-Axir [100]studied the residual stress profile with increasing depth beneath the machined surface of steel, aluminum, and brass parts

Table 4
Material, process, and parameter information for Fig. 49.

Reference	Work material	Tool material	Process	Parameters	Remarks
Ezugwu et al. [30]	IN-718	Coated carbide (TiN and TiN/TiCN//TiN PVD-coated, TiC/Al_2O_3/TiN CVD-coated)	Turning	V=32–56 m/min f=0.13, 0.25 mm/rev d=1, 2mm	Microhardness values at the surface increased slightly with increasing depth of cut
Darwish [31]	IN-718	Ceramic and CBN	Turning	V=32,125 m/min f=0.075–0.6 mm/rev d=0.5,2 mm	As depth of cut increased, surface quality decreased
Sridhar et al. [16]	Ti-IMI 834	Coated carbide (TiN)	Milling	V=11–56 m/min f=0.056–0.1 mm/tooth d=0.25–2 mm	The compressive magnitude of residual stresses decreased when depth of cut was increased
Arunachalam et al. [35]	IN-718 (36 HRC)	CBN and mixed ceramic	Facing	V=150–450 m/min f=0.15 mm/rev DoC=0.05–0.5 mm	With increasing depth of cut, residual stresses become less compressive at 5 mm from the periphery and more tensile at 25 mm from the periphery
Pawade et al. [48]	IN-718	PCBN	Turning	V=125, 300, 475 m/min f=0.05, 0.1, 0.15 mm/rev DoC=0.5, 0.75, 1 mm	As depth of cut increased, residual stresses change from tensile to compressive. Also, higher depth of cut resulted in significantly higher microhardness at the surface
Sun and Guo [10]	Ti-64	Coated carbide (TiAlN)	End milling	V=50–110 m/min f=0.06–0.14 mm/tooth d=1.5 mm	Surface of the material became rougher when the depth of cut increased due to increased overlap between cutting paths

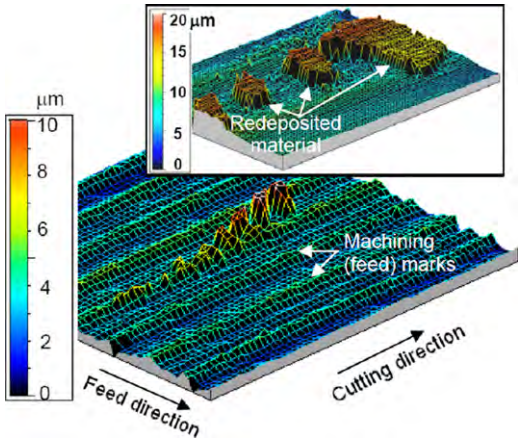

Fig. 50. Meshed profile of the surface [43].

using the cutting speed, feed rate, and the tensile strength of the material. Capello [95] proposed a regression equation with inputs feed rate (f), tool nose radius (r) and entrance angle (χ) to find the residual stresses (σ_r) on the UNI-ISO Fe370, C45, and 39NiCrMo3 steels, where k_i's are empirical equation coefficients:

$$\sigma_r = 1000\log\left(k_1 f^{k_2} f^{k_3}\right) - k_4\chi \tag{5}$$

Moreover, Shi et al. [99] expressed the white layer thickness (t_w) as a linear equation with input parameters of coolant existence (C_l), flank wear (V_b), cutting speed (U), rake angle (γ), tool nose radius (R), feed rate (f), tool thermal conductivity (K_{tl}) in turning AISI 52100 steel:

$$t_w = \beta_0 + \beta_1 C_l + \beta_2 V_b + \beta_3 U + \beta_4\gamma + \beta_5 R + \beta_6 f + \beta_7 K_{tl} + \varepsilon \tag{6}$$

They found that this equation did not satisfactorily capture the relationship between the input parameters and the white layer thickness. So, they proposed a linear equation with square root transformation where white layer thickness was denoted as t_w, and another model with second-order terms, where white layer thickness is shown with y and input parameters with x_i's:

$$t_w^{1/2} = \beta_0 + \beta_1 C_l + \beta_2 V_b^{1/2} + \beta_3 U^{1/2} + \beta_4\gamma^{1/2} + \beta_5 R^{1/2} + \beta_6 f^{1/2} + \beta_7 K_{tl}^{1/2} + \varepsilon$$

$$y = \beta_0 + \sum_{i=1}^{7}\beta_i x_i + \sum_{i=2}^{3}\beta_{ii}x_i^2 + \sum_{i=1}^{7}\sum_{j=1}^{7}\beta_{ij}x_i x_j + \varepsilon \tag{7}$$

The general finding of these studies is that depending on the experiments, the output parameters can be found to depend heavily or slightly on the input parameters, but the only general consensus is that the cutting speed and feed rate are the most effective parameters on residual stresses and surface roughness. These methods generally provide the ability to model the processes that cannot be measured or analytically predicted easily, the processes that are generally seen as 'black boxes'. The researchers have tried to model the residual stresses and white layer thicknesses according to the process parameters and tool geometry and wear, as well as workpiece material properties, and found some relations in terms of these parameters and coefficients they found through experimentation. However, these methods do not provide physical means of explanation to the processes and the results, which is the missing part of these findings. Thus, some researchers sought better means of physical explanation using analytical and FEM-based methods.

4.3. Analytical modeling techniques

Among all types of methods of analysis, analytical form is the most difficult method to achieve, since there are many unknowns to the processes, and these unknowns need to be solved either by the help of other methods, or through assumptions. When a large number of assumptions are made, the researcher faces the threat of becoming distant from modeling what is actually happening during

the process, and when these assumptions are withheld, modeling becomes harder. However, due to the fact that these methods are more physics-based rather than experimental modeling, they can reflect the actual physical phenomenon better than the other methods. Hence, other than the issue about assumptions, these methods are the closest a researcher can get to the solution of the actual problem.

The analytical formulations of surface integrity parameters such as residual stress, surface roughness, hardness and white layer depth are only common for steel materials, and not very widespread for nickel and titanium alloys. However, the information gathered from the analytical formulations for steel materials can be used as a guideline to investigate the analytical solutions for nickel and titanium alloys. There is a scarcity of studies in the analytical formulation of nickel and titanium alloys, so using the methods that are well-established for steel materials can be the starting point. Therefore, analytical models offered for steel surface integrity studies will be briefly discussed here.

Chou and Evans [78] proposed a thermal model that relates the critical temperature penetration depth to dimensionless white layer depth, resulting in the white layer depth prediction, given that the penetration depth is known accurately. They validated their model with experimental results for hard turning AISI 52100 steel. However, this model has many assumptions in it that these assumptions make the case far away from the real case, and the accuracy of the prediction of white layer depth is also compromised. Assuming that the flank wear is constant, they suggested that the white layer thickness (z_{cr}) is only a function of cutting speed (V), where VB is the average flank wear land width:

$$\frac{2z_{cr}}{VB} = \text{Function of cutting speed, } V \tag{8}$$

Chou and Song [102] developed this thermal model with less assumptions and showed that rake face temperatures, hence the temperature on the grid in general, increase with cutting speed and feed rate, but decrease with depth of cut. Since the temperature has a great effect on surface integrity of the end product, including the white layer formation and residual stresses, predicting the temperatures or accurately measuring them, and knowing how they would be with changing process parameters is crucial. They started with prediction of forces applied on the workpiece:

$$F = f(r,\alpha_0,i,c,A_c,K_n,K_f,\theta,L) \tag{9}$$

In this function, F is the cutting force array, r is the tool nose radius, α_0 is the nominal rake angle, i is the inclination angle, c is the tool chamfer angle, A_c is the uncut chip area, K_n and K_f are specific normal and frictional pressures, θ is the angle variable that determines the location of the cutting edge, and L is the contact length between tool and the workpiece. Then, they continued with a thermal model that includes shear plane and rake face heat sources:

$$T = f(T_0,Q,k,l_s,l_r,\phi,\alpha,V,\chi,h_\theta) \tag{10}$$

Here, T_0 is the room temperature, Q is the heat flux, k is the thermal conductivity of the workpiece, l_s is the shear plane length, l_r is the tool-chip contact length, ϕ is the shear angle, α is the rake angle, V is the cutting speed, χ is the thermal diffusivity, and h_θ is the uncut chip thickness.

They utilized these models in order to predict the white layer thickness, although they did not supply formulation for this part.

Ulutan et al. [89] also created an analytical elasto-plastic model in order to predict the residual stresses in machining for any material, and verified their results with experimental measurements from AISI 52100 steel. Their model is based on a finite difference analysis using the cutting forces and the temperature grid for chip, tool, and the workpiece calculated as a whole at once. They included the effects of body forces, tensile surface traction, hydrostatic pressure, as well as normal compressive pressure and tangential traction, and combined the effects of these for every nodal point in the workpiece grid:

$$\begin{aligned}
\sigma_{xx}^{el} &= \sigma_{xx}^{mech} + \sigma_{xx}^{therm} \\
\sigma_{zz}^{el} &= \sigma_{zz}^{mech} + \sigma_{zz}^{therm} \\
\sigma_{xz}^{el} &= \sigma_{xz}^{mech} + \sigma_{xz}^{therm} \\
\sigma_{yy}^{el} &= \nu\left(\sigma_{xx}^{el} + \sigma_{zz}^{el}\right) - \alpha E T \\
\sigma_{ij}^{mech} &= f(z,x,f_r,f_t) \\
\sigma_{ij}^{therm} &= f(z,x,\alpha,T,E,\upsilon,G)
\end{aligned} \tag{11}$$

Here, z is the depth of the location under investigation, x is the distance in cutting speed direction between the location under investigation and the tool-workpiece contact point, f_r is the radial cutting force, f_t is the tangential cutting force, α is the thermal expansion coefficient of the workpiece, T is the temperature, E is the Young's Modulus of the workpiece, υ is the Poisson Ratio, and G is the array of plain strain Green's function values. Then, they applied the plastic deformation procedure, and used a relaxation procedure to simulate the residual stresses iteratively. They compared their results to a previously reported experiment and found out that their results matched the experimental findings in good accuracy. The peak compressive residual stresses and the changing point from tensile to compressive residual stresses were predicted with better accuracy compared to the surface tensile residual stresses, and the leveling depth for the residual stresses are not well-predicted, probably due to the noisy measurements at that level of depth.

A few studies are reported for nickel-alloy machining-induced surface integrity. Pawade et al. [53] investigated the specific shear energy of the workpiece material in machining IN-718 using an elastic–viscoplastic analytical model they created, and found out that shear band spacing increases with increasing feed rate:

$$\Delta y = \chi_1\left(\frac{mf\sin\phi_n}{\beta\cos\gamma_n}\right) \tag{12}$$

Here, χ_1 is a Taylor–Quinney coefficient showing the fraction of plastic work converted into heat, β is a flow localization parameter, m is a material constant, f is the feed, ϕ_n is the normal shear angle, and γ_n is the normal rake angle. Their results are in good agreement with experimental results.

Zhang et al. [42] used the same material (IN-718) in order to create an analytical formulation for strain rate in terms of the stress (σ), temperature (T), and the activation energy (Q), as well as the material parameter A, gas constant R, and another constant α, which can be used to represent the strain generation in machining that will be followed by hardness and white layer predictions:

$$\dot{\varepsilon} = A\exp\left(-\frac{Q}{RT}\right)\left[\sinh\alpha\sigma\right]^{1/m} \tag{13}$$

Österle and Li [57] also modeled the thermal response of the nickel-based superalloy IN-738LC upon grinding as well as its mechanical response in order to investigate the white layer formation and the contributions of mechanical and thermal responses. They found that mechanical loads and the plastic deformation associated with these loads cannot be the only reason for white layer formation, and a thermal process involving local melting of the material and rapid quenching must also have a significant effect.

In summary, the analytical solution is possible to achieve, but it is difficult, so not too many researchers deal with it. The machining processes induce forces on the machined workpieces, and these forces create heat through shearing and friction. These thermal and

mechanical loads cause the material to deform plastically and these plastic deformations, as well as the phase transformations in the material surface cause a work hardening layer in the part that has a higher hardness value than the bulk material. As a future work, it is suggested that residual stresses, hardness, surface roughness, the depth of plastic deformation, and the depth of work hardening layer may be found through the analytical formulation of these processes.

4.4. FEM-based techniques

The finite element method (FEM) based simulation techniques offer good predictions without the necessity of doing a series of experiments. The capability of these methods provide the ability to predict residual stresses and white layer formations, and the capability of these methods provide the ability to change process parameters and repeat the analysis in order to measure the sensitivity of processes to certain parameters. However, FEM-based simulations can take excessive amounts of time that they need to be optimized most of the time. Their predictions are generally close to the experimental values, especially in the measurement of residual stresses once an accurate material constitutive model is known. For this reason, FEM-based simulation models continuously focus on calibrating material constitutive model (often the Johnson–Cook material model) parameters or flow stress data using experimental results and simulation outputs.

With the use of better material constitutive models and elasto-viscoplastic deformations combined with the FEM, computational software has become available to obtain solutions for a rich set of field variables, providing much detailed insight for the chip formation processes. These FEM-based simulation techniques offer a detailed analysis of the physical process variables based on continuum mechanics principles on computational ground; hence they are fairly accurate in representing the physical phenomenon that take place during machining processes. The downside of these techniques is the computational time required to simulate a short machining time (or cutting distance) in each machining condition, which is becoming lesser of an issue with technological advancements in modern computational capabilities.

Utilizing these simulation in 2D analysis, it is possible to predict the distributions of strains, temperatures and stresses, and residual stresses after relaxation [5,72,90,96,97,103–106], and white layer thickness [56,104,107]. These predictions generally use elastic, plastic, elastic–plastic, or elastic–viscoplastic models in order to simulate the machining conditions in best way, and they use 2D orthogonal cutting results in their models, as well as workpiece and tool material properties.

Since most of industrial machining operations can be defined as 3D operations, the spatial calculation of field variables such as strain, stress and temperature in 3D chip formation should be provided fairly accurately in order to predict realistic fields for residual stresses, microhardness and white layer formation on the machined workpiece or possible wear and damage zones on the cutting tool. During the last decade, a major development in 3D FE models for machining has occurred with the advances in computers and numerical methods. Some of these models are based on the chip formation using damage criteria [108–110] for material separation or automatic techniques for remeshing of the workpiece [111,112]. Therefore, most of the recent studies are mainly focused on 3D analysis although some computational challenges remain unsolved.

FEM-based simulation models have long been suffering from the difficulty of creating a chip that separates from the workpiece and depend upon artificial chip separation methods. Most notably, Updated Lagrangian FE formulations with remeshing have been offered [111] to simulate material plastic flow around the tool tip for continuous and segmented chip formation to avoid using an artificial material separation criterion lead in developing these techniques which simplified the mechanism of material separation (chip formation). In the mean time, other models have been created which use the Arbitrary Lagrangian Eulerian (ALE) formulation for chip formation in both 2D plane strain orthogonal cutting [90,113,114] and 3D oblique cutting and turning [105,108–110,112,115] thereby advancing the state-of-the-art towards more realistic FE models for practical industrial machining operations.

Cutting force, temperature, residual stress and white layer thickness predictions have been presented in machining alloy steels such as AISI 1045 [103], AISI 316 [47,96,116], AISI 52100 [104–108], AISI 4340 [90]. These studies present fairly accurate predictions of residual stress and white layer thickness in steel machining, especially in hard turning of AISI 52100 steel.

In machining Ti-64 titanium alloy, chip formation, distributions of temperatures and stresses are obtained [5,117,118,123]. Chen et al. [5] investigated residual stress predictions using ABAQUS FE software used the Johnson-Cook model and its damage model for segmental (or serrated) chip formation. They also investigated the effects of chip formation predictions on the residual stress predictions and concluded that the predictions using the damage module for segmental chips improved the residual stress predictions. Calamaz et al. [117] developed a modified material model for Ti-64 alloy that includes strain softening for prediction of serrated chip formation. Özel et al. [118] also developed a modified material model with temperature-dependent flow softening model for Ti-64 alloy and investigated effects of tool coatings on the forces, and distributions of temperatures, stresses and tool wear rate during serrated chip formation using elasto-viscoplastic 2D and visco-plastic 3D simulation models. In literature, there exist no other predictions of residual stresses and microstructural alteration for titanium alloys made with FEM-based simulations.

FEM-based simulations are also used to investigate machining of nickel-based alloys. Most of these studies dealt with developing expertise. Sievert et al. [119] utilized the Johnson-Cook constitutive model [120] to simulate high speed machining of IN-718 nickel alloy and provided a ductile damage model. Mitrofanov et al. [39,121] have studied FE simulation of machining IN-718 nickel alloy under ultrasonic assisted turning conditions. Uhlmann et al. [46] also utilized the Johnson-Cook material model to simulate cutting of IN-718 and used model parameters proposed by Sievert et al. [119]. They have also compared simulation results from FEM software ABAQUS-2D, ABAQUS-3D and DEFORM-2D, where a ductile damage model for material separation was implemented in ABAQUS. Lorentzon et al. [51] investigated chip formation and temperatures in orthogonal cutting of IN-718. Lu and Guo [52] used 2D FEM model to investigate chip formation in multi-pass machining of IN-718. Özel [84] developed the modified Johnson-Cook material model with flow softening and a damage model to simulate chip formation and predict reliable temperature and stress fields in machining of IN-100 nickel-based alloy. Ranganath et al.[56] investigated prediction of white layer formation in IN-718 nickel-based alloy using FEM analysis and suggested that further studies are needed to develop accurate and reliable FEM models.

5. Tool materials

There are many different tool materials used in machining various titanium and nickel-based alloys, and carbides, both coated and uncoated, are the most frequently used ones in industry. Polycrystalline diamond (PCD) and cubic-boron-nitride (CBN) tools have also been widely used in machining workpiece materials that are harder to machine, and ceramic tools have been produced in

order to meet the need for different properties in tool materials. Also, the shape of the tool and edge preparation are found to be very important in the outcomes of machining processes, where round tools that had modified cutting edges were shown to exhibit lower rake face temperatures than other shapes (square and rhombic) while creating higher compressive surface layers and lower surface roughness [36].

5.1. Uncoated and coated carbides

Cemented carbides (WC/Co) are widely used in the industry; both uncoated and coated. There are various coating materials such as titanium-based TiN, TiC, TiCN and TiAlN, and others such as Al_2O_3 [122]. The reason for using coatings in these tools is to protect the tool from wear and to keep its properties intact. However, it is observed in most cases that the coating material wears out almost immediately, revealing the tool material to the process. The flank wear was found to be the most effective reason for tool failure in both uncoated and coated carbides [12]. However, it was still observed that uncoated tools reach higher maximum process temperature than coated tools [93]. These coating materials are applied on the tool by using different techniques, most common ones being chemical vapor deposition (CVD) and physical vapor deposition (PVD), where CVD is less costly but PVD provides better coating properties [122]. Ezugwu et al. [30] also reported that multi-layer PVD-coated carbide tools gave better tool life performance than single-layer PVD-coated carbide tools as well as multi-layer CVD-coated tools during turning of IN-718 at V=32–56 m/min, f=0.13–0.25 mm/rev, and DoC=1–2 mm, mostly because they have higher hardness, toughness, abrasion resistance, and good heat transmission behavior.

The workpiece material is also very effective in selection of coating material and whether to use it. Using coated carbide tools, it is shown that lower maximum tool temperature, surface stresses, and smoother chip formation were observed for steel workpieces [93], which can be effective in white layer formation, residual stresses and thickness of the work-hardened zone. However, it was observed while machining titanium alloys used in the aerospace industry that the coating materials rapidly fail because of plastic deformations and high temperatures are created during machining, so they did not make any changes to the choice of using carbide tools while machining titanium alloys [21]. This failure was mainly due to coating delamination phenomenon [14,27], proven by the use of different types of coating materials. It was shown elsewhere [12] that with or without coating, the titanium alloys form TiC material that cause the delamination of the tool material, and this delamination is increased when a multi-layer CVD-coated TiN/TiC/TiCN coating is applied. However, with the coating, it was observed that the increased chemical reaction with the coating brings smoother wear on the tool, which increases the surface quality as well as the tool life [12]. Single-layer PVD-coated (TiN) IN-718 was found to perform better in terms of surface quality compared to multi-layer CVD- and PVD-coated carbide tools during turning IN-718 at V=32–56 m/min, f=0.13–0.25 mm/rev, and DoC=1–2 mm, while multi-layer PVD-coated carbide tool had the best tool life of the three owing to its high hardness, toughness, abrasion resistance, and the thickness of the coating [30]. The uncoated carbide tool had half the tool life during turning IN-718 at V=40–120 m/min, f=0.15–0.25 mm/rev, DoC=0.25 mm compared to multi-layer coated carbide tools, and the surface roughness of the coated tool was lower as well [1]. When compared with ceramic tools with negative rake angle, PVD-coated carbide tools were only recommended because of their lower cost, but ceramic tools provided better performance in terms of tool wear and material removal rate, while turning IN-718 at V=50–300 m/min. f=0.2 mm/rev, and DoC=0.4 mm [32]. Even for some steel workpieces, some coating materials prove to be disadvantageous because they increased the tool wear rather than decreasing it due to overheating caused by extra friction they bring [73], changing the heat affected zones and therefore the white layer characteristics.

5.2. Polycrystalline diamond (PCD)

The usage of diamond itself as a coating material is limited, as it reacts with metallic and ferrous workpieces, despite the advantage of having high hardness, low friction coefficient, high thermal conductivity and low thermal expansion coefficient [122]. However, the usage of polycrystalline diamond (PCD) tools has been growing because of their performance in producing better surfaces. In addition, they are claimed to have lower wear rates compared to PCBN tools and coated carbide tools while machining titanium [8,21,23,72]. The quality of the machined product is comparable to results of polishing operations, and at the cutting speeds that the carbide tools wear out, the wearing of PCD tools is found to be significantly low [8].

5.3. Cubic-boron-nitride CBN

Cubic-boron-nitride (CBN) tools and coatings are more commonly used, because of their lower wear rates, higher hardness and strengths, good thermal conductivity, and superior mechanical properties to carbide tools [72]. They have higher hardness values than coated carbide tools, so they are more favorable in machining hard materials [122], as well as thermal crack resistance [7] that allows machining under higher temperatures observed in titanium machining, and better chemical reactivity to make better surface finishes possible on the end product [21]. They create higher cutting forces than the carbide tools, but despite of this, they are more wear resistant compared to their carbide counterparts [50]. These tools are shown to reach less tensile residual stresses compared to ceramic tools when they are used in facing of IN-718 at V=150–375 m/min, f=0.15 mm/rev, and DoC=0.5 mm [35]. However, even CBN tools are reported to deform (chipping) during machining titanium and cutting performance is affected due to this, so using lower feed rates is suggested in order to decrease tool wear and enhance surface quality [19], and Sharman et al. [1] also suggest that decreasing feed rate from 0.25 to 0.15 mm/rev slightly increased tool life. The PCBN tools were found to show higher temperature compared to ceramic tools [36]. Elsewhere [31], it was shown that CBN tools had an unfavorable effect on surface roughness when compared with ceramic tools at both low and high feed rates during turning at V=32–125 m/min, f=0.15–0.6 mm/rev, DoC=0.5–2 mm. CBN tools are still observed to wear out extensively, from sharp edge to rounded edge and even further, but experiments showed that binderless CBN (BCBN) tools had much better results while staying sharp rather than becoming rounded [23]. These different types of CBN tools such as binderless CBN tools have higher hardness and strength, higher thermal conductivity and shock resistance compared to regular CBN tools [7]. These types of tools are recommended due to their improved tool life, ability to provide better surface finish, and lower cutting forces they provide, but they are more costly compared to carbide inserts [23]. It was argued that with increased tool life, the cost can be considered to go down in the long run, making these tools more advantageous [23].

As a summary of the literature, it can be observed that in terms of surface roughness, plastic deformations, surface defects, residual stresses and the white layer formation, coatings do not provide significant advantages over non-coated carbide tools during titanium and nickel alloy machining, although some improvement in tool life and wear mechanisms (build up formation and abrasive wear) as well as achievable cutting speed was observed [35,48,54]. The PVD and CVD coatings do not show significantly advantageous

results in terms of the surface integrity properties, and the main differences in these experiments result from the material and process parameters. Tool coatings generally wear very quickly due to coating delamination phenomenon so that the coating properties cannot be used anyway, and sometimes existence of these coatings might even cause other surface problems such as carbide cracking and chemical reactions or increase the amount of tool wear. Also, they are reported to create tensile residual stresses at higher cutting speeds, compared to the compressive residual stresses produced by uncoated carbide tools at higher cutting speeds [34,35]. The main advantage of carbide tools is that they have higher resistance to crater wear. However, the achievable surface cutting speeds with carbide tools are lower (<100 m/min), whereas with ceramic tools it is possible to achieve higher cutting speeds up to 300 m/min. These ceramic tools show sudden notch wear and shorter tool life limitations, and when the higher cutting speeds are achieved, microhardness and depth of plastic deformation are reported to increase using these tools. Ceramic and cBN tools show excessive wear rates due to high chemical reactivity, so they show poor machining performance with nickel-based alloys [26,34]. Hence, despite their low achievable cutting speed, because of the surface integrity concerns in the industry, uncoated carbide tools are utilized at relatively low cutting speeds (30 m/min–60 m/min) in finishing operations for nickel-based alloyed mission critical aerospace engine components [1,34].

6. Conclusions

The quality and performance of a product is directly related to surface integrity achieved by final manufacturing process. Surface integrity includes the mechanical properties (residual stresses, hardness etc.), metallurgical states (phase transformation, microstructure and related property variations, etc.) of the work material during processing and topological parameters (surface finish and other characteristic surface topographical features). This review paper provides an overview of machining induced surface integrity in titanium and nickel alloys. The following are the specific conclusions reached in this review.

- Titanium and nickel-based alloys are becoming very popular due to their superior material properties such as low density, high strength at elevated temperatures, high corrosion resistance, high creep resistance, high toughness and durability, and high biological compatibility (titanium-based alloys), and high heat-resistance, good mechanical and chemical properties at elevated temperatures, high melting temperatures, high corrosion resistance, resistance to thermal fatigue, thermal shock, creep, and erosion (nickel-based alloys).
- Surface integrity is important in applications such as aerospace and power industries, as well as biomedical applications.
- Main surface defects observed during machining titanium- and nickel-based alloys are surface drag, material pull-out/cracking, feed marks, adhered material particles, tearing surface, chip layer formation, debris of microchips, surface plucking, deformed grains, surface cavities, slip zones, laps (material folded onto the surface), and lay patterns.
- During machining these alloys, the microstructure of the sub-surface of the bulk material is altered due to plastic deformations and white layer formation. A significant white layer, as well as a dark layer is observed during machining steel materials, but during machining titanium and nickel-based alloys, they are less visible, but in the similar pattern of finer and equiaxed grains.
- Also during machining, the surface and immediate sub-surface of the material becomes harder due to work hardening occurring because of high mechanical and thermal loads on the workpiece. The hardness value of the surface is much higher than the bulk material hardness, and it takes 200–500 μm deep into the bulk material for the hardness value to level. According to numerous studies reported for various turning and milling processes under a range of cutting conditions about work-hardening effect, the general consensus is that microhardness value at the surface of the machined workpiece increases with increasing cutting speed, feed, and depth of cut, despite the fact that some results indicated insignificant changes with feed rate and depth of cut.
- In determining the surface roughness, it was found that the high temperatures occurring during machining of titanium and nickel-based alloys is the main reason for high surface roughness values. Also, the built-up layer created at the cutting location might push the tool from its original route, which would increase the roughness values. With fresh tools, surface roughness was found to be slightly higher than lightly used tools. However, as the tool wears, it is agreed upon that the surface roughness increases significantly, which is the main reason for tool change. It was also agreed upon that with increasing cutting speed, feed rate, and depth of cut, surface roughness increases in titanium and nickel-based alloys investigated herewith.
- The major agreement on machining induced residual stresses is that they become more tensile or change from compressive to tensile at the surface when cutting speed, feed rate, and depth of cut are increased, although there are non-negligible amount of researchers claiming the opposite of these ideas. The tensile residual stresses on the surface of the material are reasons for crack initiation and fatigue failure of end products, so they need to be removed or prevented.
- There are numerous analytical methods formulated to calculate the residual stresses, the surface roughness, and white layer formation, as well as hardness profiles in steel workpieces, but there is a lack of quality work that covers these bases for titanium and nickel-based alloys.
- There are many empirical models for steel machining, but titanium and nickel-based alloys are not investigated necessarily through empirical models. Empirical models can be utilized in order to have a sense in how machining parameters affect the outputs of surface integrity, but they would not be sufficient to emphasize the physical meaning of the processes.
- Finite element method based simulation models for predicting machining induced white layer formation, microhardness and residual stress profiles seem to be the most promising research approach due to the recent advances in numerical solution methods and computational power. Accurate and reliable material models for elastic–viscoplastic workpiece deformations and multi-scale models including metallurgical and microstructural behavior of those materials, and computational complexity for practical machining processes remain to be the major research challenges.
- For machining titanium- and nickel-based alloys, there are many different types of cutting tools are employed, and carbide tools are still the most commonly used materials. Coating materials are used in order to improve machining performance, and they are shown to be efficient in machining steel, but titanium and nickel-based alloys do not allow significant improvement in machining using coating materials, due to the rapid delamination problem.
- PVD- and CVD-coatings, as well as single-layer and multi-layer coatings have different advantages in machining different materials at different machining conditions, so the choice of coating materials should be process-specific.
- PCD and CBN tools are also becoming popular in the recent years, because of their higher wear resistance and hardness. However, these materials are more expensive than the carbide tools and they may not always provide better results at all conditions. The cost of the cutting tool should be calculated by considering the

amount of material removal and tool life of the materials, which might demonstrate some advantages of CBN tools in becoming more economic and efficient.

- Although some studies have been reported on the effects of tool edge geometry on machining of titanium- and nickel-based alloys, influence of tool edge micro-geometry variation on obtaining favorable machining induced residual stresses has not been explored well. Current research interests include also exploring effects of coating materials and tool edge micro-geometry by means of experimental and numerical methods.

References

[1] A.R.C. Sharman, J.J. Hughes, K. Ridgway, Workpiece surface integrity and tool life issues when turning Inconel 718 nickel based superalloy, Machining Science and Technology 8 (3) (2004) 399–414.
[2] Q. Wu, Serrated chip formation and tool-edge wear in high-speed machining of advanced aerospace materials, Utah State University, Logan, Utah, 2007.
[3] R. M'Saoubi, J.C. Outeiro, H. Chandrasekaran, O.W. Dillon Jr., I.S. Jawahir, A review of surface integrity in machining and its impact on functional performance and life of machined products, International Journal of Sustainable Manufacturing 1 (1–2) (2008) 203–236.
[4] Y.B. Guo, W. Li, I.S. Jawahir, Surface integrity characterization and prediction in machining of hardened and difficult-to-machine alloys; a state-of-the-art research review and analysis, Machining Science and Technology 13 (2009) 437–470.
[5] L. Chen, T.I. El-Wardany, W.C. Harris, Modeling the effects of flank wear land and chip formation on residual stresses, CIRP Annals—Manufacturing Technology 53 (1) (2004) 95–98.
[6] C.H. Che-Haron, A. Jawaid, The effect of machining on surface integrity of titanium, Journal of Materials Processing Technology 166 (2005) 188–192.
[7] Z.G. Wang, M. Rahman, Y.S. Wong, Tool wear characteristics of binderless CBN tools used in high-speed milling of titanium alloys, Wear 258 (2005) 752–758.
[8] A.K.M. Nurul-Amin, A.F. Ismail, M.K. Nor Khairusshima, Effectiveness of uncoated WC-Co and PCD inserts in end milling of titanium alloy—Ti–6Al–4V, Journal of Materials Processing Technology 192–193 (2007) 147–158.
[9] S. Sun, M. Brandt, M.S. Dargusch, Characteristics of cutting forces and chip formation in machining of titanium alloys, International Journal of Machine Tools and Manufacture 49 (2009) 561–568.
[10] J. Sun, Y.B. Guo, A comprehensive experimental study on surface integrity by end milling Ti-6Al-4V, Journal of Materials Processing Technology 209 (2009) 4036–4042.
[11] M. Thomas, S. Turner, M. Jackson, Microstructural damage during high-speed milling of titanium alloys, Scripta Materialia 62 (2010) 250–253.
[12] C.H. Che-Haron, A. Ginting, H. Arshad, Performance of alloyed uncoated and CVD-coated carbide tools in dry milling of titanium alloy Ti-6242S, Journal of Materials Processing Technology 185 (2007) 77–82.
[13] A. Ginting, M. Nouari, Optimal cutting conditions when dry end milling the aeroengine material Ti-6242S, Journal of Materials Processing Technology 184 (2007) 319–324.
[14] A. Ginting, M. Nouari, Surface integrity of dry machined titanium alloys, International Journal of Machine Tools and Manufacture 49 (2009) 325–332.
[15] C.H. Che-Haron, Tool life and surface integrity in turning titanium alloy, Journal of Materials Processing Technology 118 (2001) 231–237.
[16] B.R. Sridhar, G. Devananda, K. Ramachandra, R. Bhat, Effect of machining parameters and heat treatment on the residual stress distribution in titanium alloy IMI-834, Journal of Materials Processing Technology 139 (2003) 628–634.
[17] A.L. Mantle, D.K. Aspinwall, Surface integrity and fatigue life of turned gamma titanium aluminide, Journal of Materials Processing Technology 72 (1997) 413–420.
[18] A.L. Mantle, D.K. Aspinwall, Surface integrity of a high speed milled gamma titanium aluminide, Journal of Materials Processing Technology 118 (2001) 143–150.
[19] Z.A. Zoya, R. Krishnamurty, The performance of CBN tools in the machining of titanium alloys, Journal of Materials Processing Technology 100 (2000) 80–86.
[20] T. Kitagawa, A. Kubo, K. Maekawa, Temperature and wear of cutting tools in high-speed machining of Inconel 718 and Ti–6Al–6V–2Sn, Wear 202 (1997) 142–148.
[21] F. Nabhani, Machining of aerospace titanium alloys, Robotics and Computer Integrated Manufacturing 17 (2001) 99–106.
[22] W.F. Cui, Z. Jin, A.H. Guo, L. Zhou, High temperature deformation behavior of $\alpha+\beta$-type biomedical titanium alloy Ti–6Al–7Nb, Materials Science and Engineering A 499 (2009) 252–256.
[23] M. Rahman, Y.S. Wong, A.R. Zareena, Machinability of titanium alloys, JSME Series C 46 (1) (2003) 107–115.
[24] A.B. Sadat, Surface region damage of machined Inconel 718 nickelbase superalloy using natural and controlled contact length tools, Wear 119 (1987) 225–235.
[25] A.B. Sadat, M.Y. Reddy, B.P. Wang, Plastic deformation analysis in machining of Inconel 718 nickel base superalloy using both experimental and numerical methods, International Journal of Mechanical Sciences 33 (10) (1991) 829–842.
[26] E.O. Ezugwu, S.H. Tang, Surface abuse when machining cast iron (G-17) and nickel-base superalloy (Inconel 718) with ceramic tools, Journal of Materials Processing Technology 55 (1995) 63–69.
[27] Y.S. Liao, R.H. Shiue, Carbide tool wear mechanism in turning of Inconel 718 superalloy, Wear 193 (1996) 16–24.
[28] S. Derrien, J. Vigneau, High speed milling of difficult to machine alloys, in: D. Dudzinski, A. Devillez, A. Moufki, D. Larrouquerre, V. Zerrouki, J. Vigneau (Eds.), A review of developments towards dry and high speed machining of Inconel 718 alloy, International Journal of Machine Tools and Manufacture 44 (2004) 439–456.
[29] M. Rahman, W.K.H. Seah, T.T. Teo, The machinability of Inconel 718, Journal of Materials Processing Technology 63 (1997) 199–204.
[30] E.O. Ezugwu, Z.M. Wang, C.I. Okeke, Tool life and surface integrity when machining Inconel 718 with PVD and CVD coated tools, Tribology Transactions 42 (2) (1999) 353–360.
[31] S.M. Darwish, The impact of tool material and the cutting parameters on surface roughness of supermet 718 nickel superalloy, Journal of Materials Processing Technology 97 (2000) 10–18.
[32] L. Li, N. He, M. Wang, Z.G. Wang, High speed cutting of Inconel 718 with coated carbide and ceramic inserts, Journal of Materials Processing Technology 129 (1–3) (2002) 127–130.
[33] C. Schlauer, R.L. Peng, M. Oden, Residual stresses in a nickel-based superalloy introduced by turning, Material Science Forum 404–407 (2002) 173–178.
[34] M. Arunachalam, M.A. Mannan, A.C. Spowage, Surface integrity when machining age hardened Inconel 718 with coated carbide cutting tools, International Journal of Machine Tools and Manufacture 44 (2004) 1481–1491.
[35] R.M. Arunachalam, M.A. Mannan, A.C. Spowage, Residual stress and surface roughness when facing age hardened Inconel 718 with CBN and ceramic cutting tools, International Journal of Machine Tools and Manufacture 44 (2004) 879–887.
[36] R.T. Coelho, L.R. Silva, A. Braghini Jr., A.A. Bezerra, Some effects of cutting edge preparation and geometric modifications when turning Inconel 718 at high cutting speeds, Journal of Materials Processing Technology 148 (1) (2004) 147–153.
[37] L. Guerville, J. Vigneau, Influence of machining conditions on residual stresses, in: D. Dudzinski, A. Devillez, A. Moufki, D. Larrouquerre, V. Zerrouki, J. Vigneau (Eds.), A review of developments towards dry and high speed machining of Inconel 718 alloy, International Journal of Machine Tools and Manufacture 44 (2004) 439–456.
[38] D. Dudzinski, A. Devillez, A. Moufki, D. Larrouquerre, V. Zerrouki, J. Vigneau., A review of developments towards dry and high speed machining of Inconel 718 alloy, International Journal of Machine Tools and Manufacture 44 (2004) 439–456.
[39] A.V. Mitrofanov, V.I. Babitsky, V.V. Silberschmidt, Finite element analysis of ultrasonically assisted turning of Inconel 718, Journal of Materials Processing Technology 153–154 (2004) 233–239.
[40] A.R.C. Sharman, J.I. Hughes, K. Ridgway, An analysis of the residual stresses generated in Inconel 718 when turning, Journal of Materials Processing Technology 173 (2006) 359–367.
[41] A.R.C Sharman, J.I. Hughes, K. Ridgway, Surface integrity and tool life when turning Inconel 718 using ultra-high pressure and flood coolant systems, Proceedings of the Institution of Mechanical Engineers, Part B: Journal of Engineering Manufacture 222 (2008) 653–664.
[42] B. Zhang, D.J. Mynors, A. Mugarra, K. Ostolaza, Representing the superplasticity of Inconel 718, Journal of Materials Processing Technology 153–154 (2004) 694–698.
[43] D.A. Axinte, P. Andrews, W. Li, N. Gindy, P.J. Withers, Turning of advanced Ni based alloys obtained via powder metallurgy route, Annals of the CIRP 55 (2006).
[44] D.K. Aspinwall, R.C. Dewes, E.-G. Ng, C. Sage, S.L. Soo, The influence of cutter orientation and workpiece angle on machinability when high-speed milling Inconel 718 under finishing conditions, International Journal of Machine Tools and Manufacture 47 (2007) 1839–1846.
[45] R.S. Pawade, S.S. Joshi, P.K. Brahmankar, M. Rahman, An investigation of cutting forces and surface damage in high-speed turning of Inconel 718, Journal of Materials Processing Technology 192–193 (2007) 159.
[46] E. Uhlmann, M. Graf von der Schulenburg, R. Zettier, Finite element modeling and cutting simulation of Inconel 718, Annals of the CIRP 56 (1) (2007) 61–64.
[47] J.C. Outeiro, J.C. Pina, R. M'Saoubi, F. Pusavec, I.S. Jawahir, Analysis of residual stresses induced by dry turning of difficult-to-machine materials, CIRP Annals—Manufacturing Technology 57 (2008) 77–80.
[48] R.S. Pawade, S.S. Joshi, P.K. Brahmankar, Effect of machining parameters and cutting edge geometry on surface integrity of high-speed turned Inconel 718, International Journal of Machine Tools and Manufacture 48 (2008) 15–28.
[49] C. Courbon, D. Kramar, P. Krajnik, F. Pusavec, J Rech, J Kopac, Investigation of machining performance in high-pressure jet assisted turning of Inconel 718: an experimental study, International Journal of Machine Tools and Manufacture 49 (2009) 1114–1125.
[50] K. Jemielniak, Finish turning of Inconel 718, Advances in Manufacturing Science and Technology 33 (1) (2009) 59–69.

[51] J. Lorentzon, N. Jarvstrat, B.L. Josefson, Modeling chip formation of alloy 718, Journal of Materials Processing Technology 209 (2009) 4645–4653.
[52] Y. Lu, C. Guo, Finite element modeling of multi-pass machining of Inconel 718, CD Proceedings of 2009 ASME International Conference on Manufacturing Science and Engineering, Paper No. 84086, Lafayette, Indiana, USA, October 5–7, 2009.
[53] R.S. Pawade, H.A. Sonawane, S.S. Joshi, An analytical model to predict specific shear energy in high-speed turning of Inconel 718, International Journal of Machine Tools and Manufacture 49 (2009) 979–990.
[54] S. Ranganath, C. Guo, S. Holt, Experimental investigations into the carbide cracking phenomenon on Inconel 718 superalloy material, ASME 2009 International Manufacturing Science and Engineering Conference, 2009.
[55] B. Zou, M. Chen, C. Huang, Q. An, Study on surface damages caused by turning $NiCr_{20}TiAl$ nickel-based alloy, Journal of Materials Processing Technology 209 (2009) 5802–5809.
[56] S. Ranganath, C. Guo, P. Hegde, A finite element modeling approach to predicting white layer formation in nickel superalloys, CIRP Annals—Manufacturing Technology 58 (2009) 77–80.
[57] W. Österle, P.X. Li, Mechanical and thermal response of a nickel-base superalloy upon grinding with high removal rates, Materials Science and Engineering A 238 (1997) 357–366.
[58] C. Cui, Y. Gu, H. Harada, A. Sato, Microstructure and yield strength of UDIMET 720LI alloyed with Co-16.9 Wt Pct Ti, Metallurgical and Materials Transactions A 36A (2005) 2921–2927.
[59] S.V. Joshi, S.P. Vizhian, B.R. Sridhar, K. Jayaram, Parametric study of machining effect on residual stress and surface roughness of nickel base super alloy UDIMET 720, Advanced Materials Research 47–50 (2008) 13–16.
[60] P.K. Wright, J.G. Chow, Deformation characteristics of nickel alloys during machining, Journal of Engineering Materials and Technology, Transactions of the ASME 104 (1982) 85–93.
[61] E.O. Ezugwu, Key improvements in the machining of difficult-to-cut aerospace superalloys, International Journal of Machine Tools and Manufacture 45 (2005) 1353–1367.
[62] J.J. Ramsden, D.M. Allen, D.J. Stephenson, J.R. Alcock, G.N. Peggs, G. Fuller, G. Goch, The design and manufacture of biomedical surfaces, Annals of the CIRP 56 (2) (2007) 687–711.
[63] W. Chrzanowski, E.Ali Abou Neel, D.A. Armitage, J.C. Knowles, Effect of surface treatment on the bioactivity of nickel–titanium, Acta Biomaterialia 4 (2008) 1969–1984.
[64] D Bogdanski, M. Epple, S.A. Esenwein, G. Muhr, V. Petzoldt, O. Prymak, K. Weinert, M. Köller, Biocompatibility of calcium phosphate-coated and of geometrically structured nickel–titanium (NiTi) by in vitro testing models, Materials Science and Engineering A 378 (2004) 527–531.
[65] K. Weinert, V. Petzoldt, Machining of NiTi based shape memory alloys, Materials Science and Engineering A 378 (2004) 180–184.
[66] K. Weinert, V. Petzoldt, Machining NiTi micro-parts by micro-milling, Materials Science and Engineering A 481–482 (2008) 672–675.
[67] K. Weinert, V. Petzoldt, D. Kötter, Turning and drilling of NiTi shape memory alloys, CIRP Annals—Manufacturing Technology 53 (1) (2004) 65–68.
[68] F. Ghanem, C. Braham, M.E. Fitzpatrick, H. Sidhom, Effect of near-surface residual stress and microstructure modification from machining on the fatigue endurance of a tool steel, Journal of Materials Engineering and Performance 11 (6) (2002) 631–639.
[69] S. Kalpakjian, S.R. Schmid, Manufacturing Processes for Engineering Materials, 5th edition, Prentice-Hall, 2007.
[70] D. Novovic, R.C. Dewes, D.K. Aspinwall, W. Voice, P. Bowen, The effect of machined topography and integrity on fatigue life, International Journal of Machine Tools and Manufacture 44 (2004) 125–134.
[71] M. Field, J.F. Kahles, W.P. Koster, Surface finish and surface integrity, USAF Technical Report AFML-TR-74-60 Metcut Research, Associates Inc., Cincinatti, OH, 1974.
[72] X. Yang, C.R. Liu, Machining titanium and its alloys, Machining Science and Technology 3.1 (1999) 107–139.
[73] A.G. Jaharah, C.H. Che Hassan, N. Muhamad, Machined surface of AISI H13 tools steels when end milling using P10 TiN coated carbide tools, European Journal of Scientific Research 26 (2) (2009) 247–254.
[74] B. Zhang, W. Shen, Y. Liu, X. Tang, Y. Wang, Microstructures of surface white layer and internal white adiabatic shear band, Wear 211 (1997) 164–168.
[75] S.S. Bosheh, P.T. Mativenga, White layer formation in hard turning of H13 tool steel at high cutting speeds using CBN tooling, International Journal of Machine Tools and Manufacture 46 (2006) 225–233.
[76] T. Connolley, P.A.S. Reed, M.J. Starink, Short crack initiation and growth at 600 °C in notched specimens of Inconel 718, Materials Science and Engineering A 340 (2003) 139–154.
[77] W. König, H.K. Tönshoff, G. Ackershott, Machining of hard materials, Annals of the CIRP 33 (2) (1984) 417–427.
[78] Y.K. Chou, C.J. Evans, White layers and thermal modeling of hard turned surfaces, International Journal of Machine Tools and Manufacture 39 (1999) 1863–1881.
[79] X. Sauvage, J.M. Le Breton, A. Guillet, A. Meyer, J. Teillet, Phase transformations in surface layers of machined steels investigated by X-ray diffraction and Mössbauer spectrometry, Materials Science and Engineering A 362 (2003) 181–186.
[80] S. Han, S.N. Melkote, M.S. Haluska, T. Watkins, White layer formation due to phase transformation in orthogonal machining of AISI 1045 annealed steel, Materials Science and Engineering A 488 (2008) 195–204.
[81] F. Hashimoto, Y.B. Guo, A.W. Warren, Surface integrity difference between hard turned and ground surfaces and its impact on fatigue life, Annals of the CIRP 55 (1) (2006) 81–84.
[82] A. Ramesh, S.N. Melkote, L.F. Allard, L. Riester, T.R. Watkins, Analysis of white layers formed in hard turning of AISI 52100 steel, Materials Science and Engineering A 390 (2005) 88–97.
[83] A.R. Machado, J. Wallbank, Machining of titanium and its alloys—a review, Proceedings of the Institution of Mechanical Engineers 204 (1990) 53–60.
[84] T. Özel, Experimental and finite element investigations on the influence of tool edge radius in machining nickel-based alloy, CD Proceedings of 2009 ASME International Conference on Manufacturing Science and Engineering, Paper No. 84362, Lafayette, Indiana, USA, October 5–-7, 2009.
[85] K. Weinert, D. Biermann, S. Bergmann, Machining of high strength light weight alloys for engine applications, Annals of the CIRP 56 (1) (2007) 105–108.
[86] D.A. Axinte, R.C. Dewes, Surface integrity of hot work tool steel after high speed milling-experimental data and empirical models, Journal of Materials Processing Technology 127 (2002) 325–335.
[87] K. Jacobus, R.E. DeVor, S.G. Kapoor, Machining-induced residual stress: experimentation and modeling, Journal of Manufacturing Science and Engineering 122 (2000) 20–31.
[88] P. Chevrier, A. Tidu, B. Bolle, P. Ccezard, J.P. Tinnes, Investigation of surface integrity in high speed end milling of a low alloyed steel, International Journal of Machine Tools and Manufacture 43 (2003) 1135–1142.
[89] D. Ulutan, B.E. Alaca, I. Lazoglu, Analytical modeling of residual stresses in machining, Journal of Materials Processing Technology 183 (2007) 77–87.
[90] T. Özel, E. Zeren, Finite element modeling the influence of edge roundness on the stress and temperature fields induced by high-speed machining, International Journal of Advanced Manufacturing Technology 35 (2007) 255–267.
[91] J. Hua, R. Shivpuri, X. Cheng, V. Bedekar, Y. Matsumoto, F. Hashimoto, T.R. Watkins, Effect of feed rate, workpiece hardness and cutting edge on subsurface residual stress in the hard turning of bearing steel using chamfer+hone cutting edge geometry, Materials Science and Engineering A 394 (2005) 238–248.
[92] D. Hua, R. Umbrello, Shivpuri, Investigation of cutting conditions and cutting edge preparations for enhanced compressive subsurface residual stress in the hard turning of bearing steel, Journal of Materials Processing Technology 171 (2006) 180–187.
[93] R. M'Saoubi, J.C. Outeiro, B. Changeux, J.L. Lebrun, A. Morão Dias, Residual stress analysis in orthogonal machining of standard and resulfurized AISI 316L steels, Journal of Materials Processing Technology 96 (1999) 225–233.
[94] P. Dahlman, F. Gunnberg, M. Jacobson, The influence of rake angle, cutting speed and cutting depth on residual stresses in hard turning, Journal of Materials Processing Technology 147 (2004) 181–184.
[95] E. Capello, Residual stresses in turning part I: influence of process parameters, Journal of Materials Processing Technology 160 (2005) 221–228.
[96] J.C. Outeiro, D. Umbrello, R. M'Saoubi, Experimental and numerical modeling of residual stresses induced in orthogonal cutting of AISI 316L steel, International Journal of Machine Tools and Manufacture 46 (2006) 1786–1794.
[97] M. Nasr, E.G. Ng, M. Elbestawi, Effects of workpiece thermal properties on machining-induced residual stresses—thermal softening and conductivity, Journal of Engineering Manufacture 221 (2007) 1387–1400.
[98] G. Poulachon, A. Albert, M. Schluraff, I.S. Jawahir, An experimental investigation of work material microstructure effects on white layer formation in PCBN hard turning, International Journal of Machine Tools and Manufacture 45 (2005) 211–218.
[99] J. Shi, J.Y. Wang, C.R. Liu, Modeling white layer thickness based on the cutting parameters of hard machining, Journal of Engineering Manufacture 220 (2006) 119–128.
[100] M.H. El-Axir, A method of modeling residual stress distribution in turning for different materials, International Journal of Machine Tools and Manufacture 42 (2002) 1055–1063.
[101] B.K. Subhas, R. Bhat, K. Ramachandra, H.K. Balakrishna, Simultaneous optimization of machining parameters for dimensional instability control in aero gas turbine components made of Inconel 718 alloy, Transactions of ASME, Journal of Manufacturing Science and Engineering 122 (2000) 586–590.
[102] Y.K. Chou, H. Song, Thermal modeling for hard turning using a new tool, ASME International Mechanical Engineering Congress (2003) 1–10.
[103] K.C. Ee, O.W. Dillon Jr., I.S. Jawahir, Finite element modeling of residual stresses in machining induced by cutting using a tool with finite edge radius, International Journal of Mechanical Sciences 47 (2005) 1611–1628.
[104] A. Ramesh, S.N. Melkote, Modeling of white layer formation under thermally dominant conditions in orthogonal machining of hardened AISI 52100 steel, International Journal of Machine Tools and Manufacture 48 (2008) 402–414.
[105] P.J. Arrazola, T. Özel, Numerical modelling of 3-D hard turning using Arbitrary Eulerian Lagrangian finite element method, International Journal of Machining and Machinability of Materials 3 (3) (2008) 238–249.
[106] Y.B. Guo, S. Anurag, I.S. Jawahir, A novel hybrid predictive model and validation of unique hook-shaped residual stress profiles in hard turning, CIRP Annals—Manufacturing Technology 58 (1) (2009) 81–84.
[107] D. Umbrello, L. Filice, Improving surface integrity in orthogonal machining of hardened AISI 52100 steel by modeling white and dark layers formation, CIRP Annals—Manufacturing Technology 58 (2009) 73–76.
[108] Y.B. Guo, C.R. Liu, 3D FEA modeling of hard turning, ASME Journal of Manufacturing Science and Engineering 124 (2002) 189–199.

[109] S.L. Soo, D.K. Aspinwall, R.C. Dewes, 3D FE modeling of the cutting of Inconel 718, Journal of Materials Processing Technology 150 (2004) 116–123.
[110] S.L. Soo, D.K. Aspinwall, R.C. Dewes Three-Dimensional, Finite element modelling of high-speed milling of Inconel 718, Proceedings of the Institution of Mechanical Engineers, Part B: Journal of Engineering Manufacture 218 (2004) 1555–1561.
[111] T.D. Marusich, M. Ortiz, Modeling and simulation of high-speed machining, International Journal for Numerical Methods in Engineering 38 (1995) 3675–3694.
[112] T. Özel, Computational modelling of 3-D turning with variable edge design tooling: influence of micro-geometry on forces, stresses, friction and tool wear, Journal of Materials Processing Technology 209 (11) (2009) 5167–5177.
[113] M.N.A. Nasr, E.-G. Ng, M.A. Elbestawi, A modified time-efficient FE approach for predicting machining-induced residual stresses, Finite Elements in Analysis and Design 44 (4) (2008) 149–161.
[114] A. Haglund, H.A. Kishawy, R.J. Rogers, An exploration of friction models for the chip tool interface using an Arbitrary Lagrangian–Eulerian finite element model, Wear 265 (3–4) (2008) 452–460.
[115] I. Llanos, J.A. Villar, I. Urresti, P.J. Arrazola, Finite element modeling of oblique machining using an Arbitrary Lagrangian–Eulerian formulation, Machining Science and Technology: An International Journal 13 (3) (2009) 385–406.
[116] M. Salio, T. Berruti, G. De Poli, Prediction of residual stress distribution after turning in turbine disks, International Journal of Machine Tools and Manufacture 44 (48) (2006) 976–984.
[117] M. Calamaz, D. Coupard, F. Girot, A new material model for 2D numerical simulation of serrated chip formation when machining titanium alloy Ti–6Al–4V, International Journal of Machine Tools and Manufacture 48 (2008) 275–288.
[118] T. Özel, M. Sima, A.K. Srivastava, B. Kaftanoglu, Investigations on the effects of multi-layered coated inserts in machining Ti–6Al–4V alloy with experiments and finite element simulations, CIRP Annals–Manufacturing Technology 59 (1) (2010) 77–82.
[119] R. Sievert, H.D. Noack, A. Hamann, P. Loewe, K.N. Singh, G. Kuenecke, R. Clos, U. Schreppel, P. Veit, E. Uhlmann, R. Zettier, Simulation der Spansegmentierung beim Hochgeschwindigkeits-Zerspanned unter Berücksichtigung duktiler Schädigung, Techniche Mechanik 23 (2–4) (2003) 216–233.
[120] G.R. Johnson, W.H. Cook, A constitutive model and data for metals subjected to large strains, high strain rates and high temperatures, Proceedings of the Seventh International Symposium on Ball (1983) 541–547.
[121] A.V. Mitrofanov, V.I. Babitsky, V.V. Silberschmidt, Thermomechanical finite element simulations of ultrasonically assisted turning, Computational Materials Science 32 (3–4) (2005) 463–471.
[122] H.G. Prengel, W.R. Pfouts, A.T. Santhanam, State of the art in hard coatings for carbide cutting tools, Surface and Coatings Technology 102 (1998) 183–190.
[123] M. Sima, T. Özel, Modified material constitutive models for serrated chip formation simulations and experimental validation in machining of titanium alloy Ti–6Al–4V, International Journal of Machine Tools and Manufacture 50 (11) (2010) 943–960. doi:10.1016/j.ijmachtools.2010.08.004.